5-27-2004

# Decadal Shifts in Biophysical Forcing of Arctic Marine Food Webs: Numerical Consequences

John J. Walsh
*University of South Florida*, jwalsh@usf.edu

Dwight A. Dieterle
*University of South Florida*

Wieslaw Maslowski
*Naval Postgraduate School*

Terry E. Whitledge
*University of Alaska*

# Decadal shifts in biophysical forcing of Arctic marine food webs: Numerical consequences

John J. Walsh and Dwight A. Dieterle
College of Marine Science, University of South Florida, St. Petersburg, Florida, USA

Wieslaw Maslowski
Department of Oceanography, Naval Postgraduate School, Monterey, California, USA

Terry E. Whitledge
School of Fisheries and Ocean Sciences, University of Alaska, Fairbanks, Alaska, USA

Received 4 May 2003; revised 26 January 2004; accepted 2 March 2004; published 27 May 2004.

[1] Fall case studies of three-dimensional circulation, plankton, and benthos models explored the consequences of interannual changes in ice cover and water motion on carbon/nitrogen cycling by the end of September within the Chukchi/Beaufort Seas. The coupled model scenarios were those of reduced (greater) northward flow, colder (warmer) temperatures, and more (less) extensive ice cover over the preceding ~60 days of August and September during the negative (positive), anticyclonic (cyclonic) phase of the Arctic Oscillation in 1980 (1989). On the inner Chukchi shelf, stronger flows in 1989 advected nitrate and silicate stocks of Pacific origin ~130 km farther northwest toward Wrangel Island than in 1980. Yet an increase of the total net photosynthesis by the diatom-dominated phytoplankton community over both shelves in 1989 was mainly the result of less ice cover of the cyclonic period, with a concomittant increase of POC influxes of phytodetritus and fecal pellets to the sediments. In terms of present shelf export, the model's separate pools of ~65 umol DOC $kg^{-1}$ and 1 ug chl $l^{-1}$, or ~4 umol POC $kg^{-1}$, at a depth of 60 m above the 2000-m isobath of the Beaufort Sea in September 1989, matched the sum of ~70 umol TOC kg-$^{-1}$ sampled there by submarine in September 1997. Accordingly, most of the simulated Chukchi shelf was a weak sink of atmospheric $CO_2$ in both September 1980 and 1989, reflecting a net fall export of particulate and dissolved debris. Within the cyclonic case of strong flows in 1989, a surface $pCO_2$ of 248 uatm was also simulated in September at 155°W on the Beaufort shelf, where ~250 uatm was measured there in September 2000. Here, farther away from the Pacific source of nutrients for enhanced photosynthesis, the model's estimate of surface sea water fugacity in a weaker flow regime was only 375 uatm of $pCO_2$ at the same location in September 1980, when typically outgassing would have instead prevailed, despite increasing atmospheric $pCO_2$ values, i.e., 356 to 362 uatm of $pCO_2$ were found in Arctic air during 1998 to 2000. Although the northward model transports of water, gases, nutrients, and particulate matter were less during 1980 than in 1989, the simulated relict nutrient fields, left behind by the model's phytoplankton on the outer shelf of the Chukchi Sea, were greater then, as a consequence of their smaller rates of light-limited utilization during less photosynthesis and draw down of $CO_2$. The more important factors, effecting fluxes of $CO_2$ here, may thus be the biological ones of photosynthesis and respiration, rather than the physical ones of temperature and advection. Since the colonial prymnesiophytes of the model also grew better at low light intensities than the diatoms or microflagellates, *Phaeocystis* won, when all other constraints were similar, in regions of the ice-covered upper euphotic zone, where total stocks were less than 0.5 ug chl $l^{-1}$, as observed in August 2000. However, increased model fidelity, compared with submarine observations of nutrients along the shelf break of the western Canadian Basin, will require appropriate specification of the persistence of winter initial conditions in Bering Strait. Future reductions of ice cover over deeper regions of these


0148-0227/04/2003JC001945

Arctic shelves may result in greater utilization of the untapped winter nutrients by these shade-adapted prymnesiophytes, with less energy transfer to higher trophic levels of their food webs. Altered bases of shelf food webs, rather than increased northward transport of Pacific waters and their constituents, may then have greater consequences for both future element cycling and protein yield of these western Arctic ecosystems. *INDEX TERMS:* 4207 Oceanography: General: Arctic and Antarctic oceanography; 4806 Oceanography: Biological and Chemical: Carbon cycling; 4817 Oceanography: Biological and Chemical: Food chains; 4842 Oceanography: Biological and Chemical: Modeling; 4845 Oceanography: Biological and Chemical: Nutrients and nutrient cycling; *KEYWORDS:* food webs, models, arctic

**Citation:** Walsh, J. J., D. A. Dieterle, W. Maslowski, and T. E. Whitledge (2004), Decadal shifts in biophysical forcing of Arctic marine food webs: Numerical consequences, *J. Geophys. Res.*, *109*, C05031, doi:10.1029/2003JC001945.

## 1. Introduction

[2] Arctic change occurs at all time scales: from diurnal tides to pre-Holocene closure of Bering Strait. As a presumed result of past anthropogenic greenhouse forcings from 1840 to 1960, however, Arctic-wide summer temperatures rose by ~1.5°C to yield the warmest habitat of the past 400 years [*Overpeck et al.*, 1997], with perhaps a consequent increase of adjacent terrestrial photosynthesis [*Myneni et al.*, 1997]. Furthermore, after more recent spring ice melt, April temperatures during 1989–1998 were 3°C warmer than in 1980–1988 [*Stabeno and Overland*, 2001] over portions of the Bering, Chukchi, and Beaufort Seas (Figure 1).

[3] Are inferred recent increases of coccolithophore abundance over the last 5 years [*Stockwell et al.*, 2001] and longer-term decreased food sources of baleen whales over the last 50 years [*Schell*, 2000, 2001] both related to altered physical habitat of temperature, ice cover, and circulation patterns on these shelves? Will future global warming first be verified in this sentinel ecosystem as altered fluxes of carbon and nitrogen between Arctic shelf and basin ecosystems? To provide a base line for a possible ice-free Arctic food web, we consider past extremes of light-regulated carbon cycling during fall in the Chukchi and Beaufort Seas with two model case studies of decadal change (Figure 2), exhibited by alternating wind fields of cyclonic and anticyclonic circulation regimes affecting ice extent, subsurface light fields, and nutrient supply.

[4] When the Beaufort High weakens and cyclonic winds above the Arctic basins intensify as a positive Arctic Oscillation (AO) index [*Thompson and Wallace*, 1998], an eastward shift in water mass boundaries has been observed [*McLaughlin et al.*, 1996] in relation to altered circulation of basin waters [*Macdonald*, 1996], warming and shallowing of the Atlantic layer [*Carmack et al.*, 1997] and a possible reduction in sea-ice extent [*Maslanik et al.*, 1996] and thickness [*McLaren et al.*, 1994; *Wadhams*, 1997]. Numerical circulation models capture both the earlier cyclonic features of the basins in the 1980s and the recent return [*Maslowski et al.*, 2001] to the anticyclonic state [*Johnson et al.*, 1999] during 1998 and 2001, when the Beaufort Gyre is stronger, the AO is negative (Figure 2a), and the Transpolar Drift retreats westward to the Lomonsov Ridge.

[5] Earlier computer models suggested anticyclonic regimes of flow in the Arctic basins (Figure 2c) during 1946–1952, 1958–1963, 1972–1979, and 1984–1988 [*Proshutinsky and Johnson*, 1997]. Over the last 30 years, the positive AO values (Figure 2a) of cyclonic periods have increased, beyond those found during 1903, such that an ice free-Arctic Ocean in summer might prevail if the trend continues [*Kerr*, 1999]. As a consequence of transition from anticyclonic to cyclonic wind patterns, the southward wind forcing above the Chukchi/Beaufort Seas is stronger in the former regime [*Zhang and Hunke*, 2001].

[6] Interannual variations in northward transport (Figure 2b) through Bering Strait of water [*Coachman and Aagaard*, 1988; *Roach et al.*, 1995], heat [*Aagaard et al.*, 2002], nutrients [*Walsh et al.*, 1989], and plankton [*Penta and Walsh*, 1995] are all linked to changes of the southward wind stress. Indeed, the strongest northward water transport over the previous 50 years was found in 1994 during the latest cyclonic period, while one of the weakest transports was observed in 1987 during the previous anticyclonic regime (Figures 2a–2c). Based on high summer temperatures in Bering Strait [*Aagaard et al.*, 2002], such strong northward transport may have occurred in 1996–1997 as well. Extensive ice cover and cold temperatures in the Bering Sea were associated with the periods of reduced northward flow during the 1970s and 1980s [*Niebauer*, 1988; *Proshutinsky and Johnson*, 1997] but not in the 1990s, impacting both the light field, the stability of the water column, and thence the base of the food web [*Stabeno and Overland*, 2001].

[7] These shifts of sea level, ice cover, surface temperatures, and storm tracks have been related to oscillations of primary production [*Sambrotto and Goering*, 1983], of zooplankton abundance [*Sugimoto and Tadokoro*, 1997], and of groundfish yields [*Hollowed and Wooster*, 1992] in the Bering Sea and by inference in the adjacent Chukchi/Beaufort Seas [*Walsh*, 1989]. However, the nitrate stocks on the outer shelf of the southeastern Bering Sea (Figure 1), found by the PROBES study (Figure 2d), did not change between anticyclonic and cyclonic periods of altered northward flow through Bering Strait [*Whitledge et al.*, 1986]. Since they are the source of nitrate exported into the Arctic from the Pacific Ocean within mainly Anadyr Water (AW) of salinity >32, after upwelling south of Bering Strait [*Walsh et al.*, 1989, 1997], the major factor of subsequent time-dependent utilization of Pacific nutrients is the residence time of phytoplankton within well-lit regions of the downstream Chukchi/Beaufort Seas.

[8] Here, we couple a relatively complex model of competition by phytoplankton and herbivores [*Walsh et al.*, 2001] to previous ones of benthic interactions [*Walsh and Dieterle*, 1994] and of water/ice motions on the

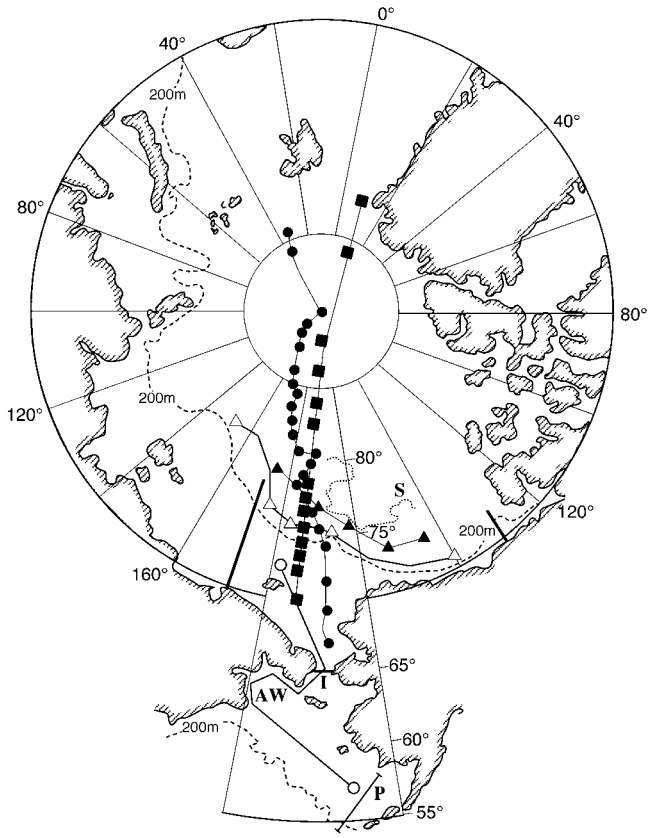


**Figure 1.** Orthogonal cruise tracks within the Arctic basins of the submarines *Pargo* (solid squares) and *Archerfish* (open triangles) during March 1991 and September 1997, as well as of the icebreakers *Polar Sea*/*Louis St. Laurent* (solid circles) and *Polar Sea*/*Henry Larsen* (solid triangles) during August 1993 and 1994 in relation to the idealized trajectory (open circles) of Anadyr Water (AW) in a prior Lagrangian model, to sites of previous PROBES (P), ISHTAR (I), SHEBA (S) programs, and to the boundaries (thick solid lines) of the coupled Eulerian SBI models.

Chukchi and Beaufort shelves [*Maslowski and Lipscomb*, 2003] for analysis of the impact of decadal changes of both ice cover and water circulation on their carbon/nitrogen exchanges with the Canadian Basin [*Walsh et al.*, 1997]. The cases of the coupled models are those of reduced (greater) northward flow, colder (warmer) temperatures, and more (less) extensive ice cover during the negative (positive), anticyclonic (cyclonic) phase of the AO in 1980 (1989) over a ~60-day period of August and September.

[9] Validation data are available both at the basin boundary (Figure 1) of this shelf ecosystem [*Guay et al.*, 1999] during other years of September 1997 (Figure 3) and on the Beaufort shelf in September 2000 [*Murata and Takizawa*, 2003], while August initial conditions of the Chukchi Sea are known from 1963 [*Codispoti and Richards*, 1968], 1968, 1969 [*Kinney et al.*, 1970], 1988 [*Walsh et al.*, 1989; *Penta and Walsh*, 1995], 1990 [*Cooper et al.*, 1997], 1993 [*Cota et al.*, 1996; *Weingartner et al.*, 1998], and 1994 [*Wheeler et al.*, 1997]. We thus assume that the Pacific summer-fall stocks of nutrients and plankton within Bering Strait remain the same from one year to the next but change seasonally, whereas those at the southern edge of the Canadian Basin are time-invariant. With extensive documentation of the circulation model, we only describe the ecological ones.

## 2. Methods

[10] A major surprise in the cyclonic year of 1997 was the first documented bloom of coccolithophores in the southeastern Bering Sea, with an associated loss of seabirds [*Stockwell et al.*, 2001]. Their contribution to alkalinity changes was considered minimal here 20 years before [*Codispoti et al.*, 1986]. They remained there in 1998 [*Hunt et al.*, 1999] and 1999 [*Olson and Strom*, 2002]. These calcareous forms can dominate the phytoplankton of Norwegian coastal waters as well [*Berge*, 1962], but they are not yet abundant farther north in the Barents Sea [*Sakshaug*, 2004].

[11] They were also not observed by AOS and SHEBA participants within the Chukchi Sea (Figure 1) during strong northward flows of either the 1994 [*Booth and Horner*, 1997] or 1997 [*Sherr et al.*, 2004] cyclonic regimes (Figure 2a). This calcium-clad functional group of phytoplankton is presently ignored, in favor of another prymnesiophyte *Phaeocystis pouchettii*, which can be important on the outer shelf of the southeastern Bering Sea [*Barnard et al.*, 1984; *Sukhanova et al.*, 1999]. It, unlike the coccolithophores, has been found within the downstream Canadian Basin as well [*Booth and Horner*, 1997; *Sherr et al.*, 2004].

[12] Diatoms tend to dominate the phytoplankton community of AW, however, whereas flagellates are more important in Alaska Coastal Water (ACW) on the eastern side of Bering Strait [*Walsh et al.*, 1989]. Both are also included as state variables, as well as their predators, copepods, and protozoans. Thus the explicit state variables of the coupled biophysical models consist of u, v, w, $K_z$, ice thickness, blue and red light, nitrate, ammonium, silicate, dissolved inorganic carbon, diatoms, microflagellates, *Phaeocystis*, copepods, protozoans, macromolecular and monomeric DOC, bacterioplankton, and sediment carbon (Table 1). Implicit variables are sediment biota, DON by Redfield ratio, and carnivorous zooplankton for food web closure.

[13] Within the water column, the processes (Table 2) of nutrient uptake and recycling, primary production and respiration, cell lysis and sinking, grazing and $CO_2$ sequestration are simulated. Across the model's sediment interface, particulate debris of uneaten phytoplankton and fecal pellets of copepod and protozoan origin is mixed down by bioturbation. Within the upper 1 cm of sediments, it is solubilized over 1 day to form lysed DOC and DON. After some oxidation to interstitial $CO_2$, the remaining DOC and biogenic DIC, as well as $NH_4$, $NO_3$, and dissolved silica of diatom frustules, outflux to the overlying water column, ignoring long-term burial [*Banahan and Goering*, 1986] over the 2-month period of the simulations. Details are provided in Appendix A.

[14] The initial and boundary conditions of AW within Bering Strait and across the inner Chukchi shelf represent ice-free, postbloom stocks of Pacific origin (Table 3), found in August, unlike larger winter amounts [*McRoy*, 1999]. In

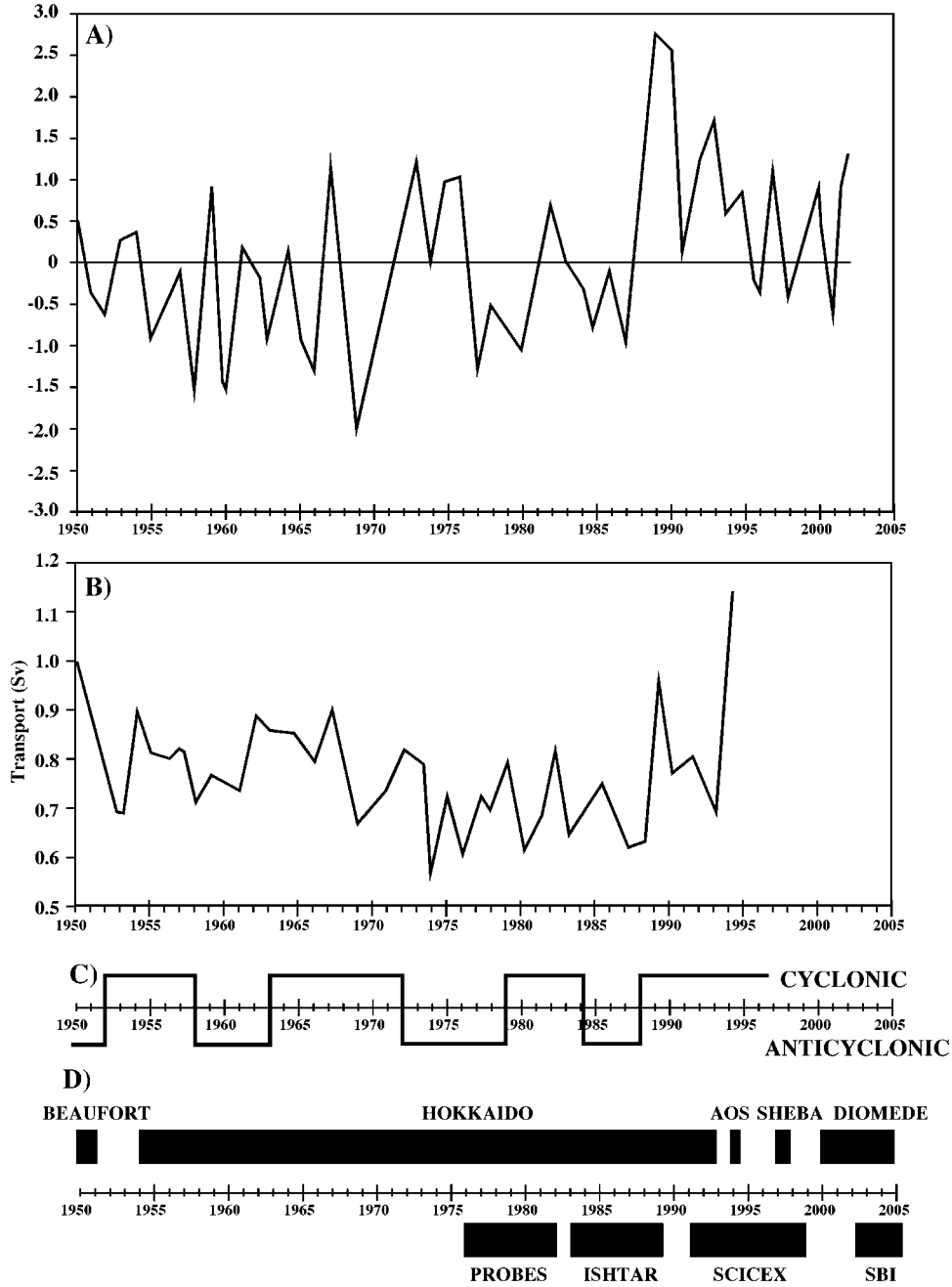


**Figure 2.** Variations of the (a) Arctic Oscillation (AO) index (available at www.cpc.ncrp.noaa.gov) and (b) northward transport through Bering Strait (after *Roach et al.* [1995]) in relation to (c) cyclonic and anticyclonic regimes of basin flows (after *Proshutinsky and Johnson* [1997]) and (d) duration of field programs over the last ~50 years of Arctic change.

contrast, those of Atlantic origin in the Canadian Basin (Table 3) are derived from submarine and ice-breaker data (Figure 1) within the pack ice [e.g., *Mumm et al.*, 1998; *Muench et al.*, 2000], but outside the influence of downstream AW, defined in the model by salinities of 32–33.5 (Figure 3a) and temperatures of −1.5°C (Figure 3b).

[15] Using these salinity fields of our physical model on 1 August, AW of 32–33.5 has initial conditions of 5–15 umol $NO_3$ $kg^{-1}$, 20–30 umol $SiO_4$ $kg^{-1}$, 0.5 umol $NH_4$ $kg^{-1}$, 0.5 ug chl $l^{-1}$ (85% diatoms; 10% prymnesiophytes; 5% microflagellates), 2050 umol DIC $kg^{-1}$, 1.0 umol C $kg^{-1}$ of copepods, protozoans, and bacteria, with a total of 90 umol DOC $kg^{-1}$ at bottom depths of 20–65 m (Table 3). Thus no attempt is made to mimic larger relict winter stocks of AW in deeper waters of the outer shelf and adjacent Canadian Basin. The boundary condition of AW in Bering Strait begins with the same initial conditions but then changes over time as a function of local biological growth and loss processes.

[16] Otherwise, over the rest of the grid of the coupled models, the initial conditions of the upper 65 m are 0.5 umol $NO_3$ $kg^{-1}$, 5.0 umol $SiO_4$ $kg^{-1}$, 0.5 umol $NH_4$ $kg^{-1}$,

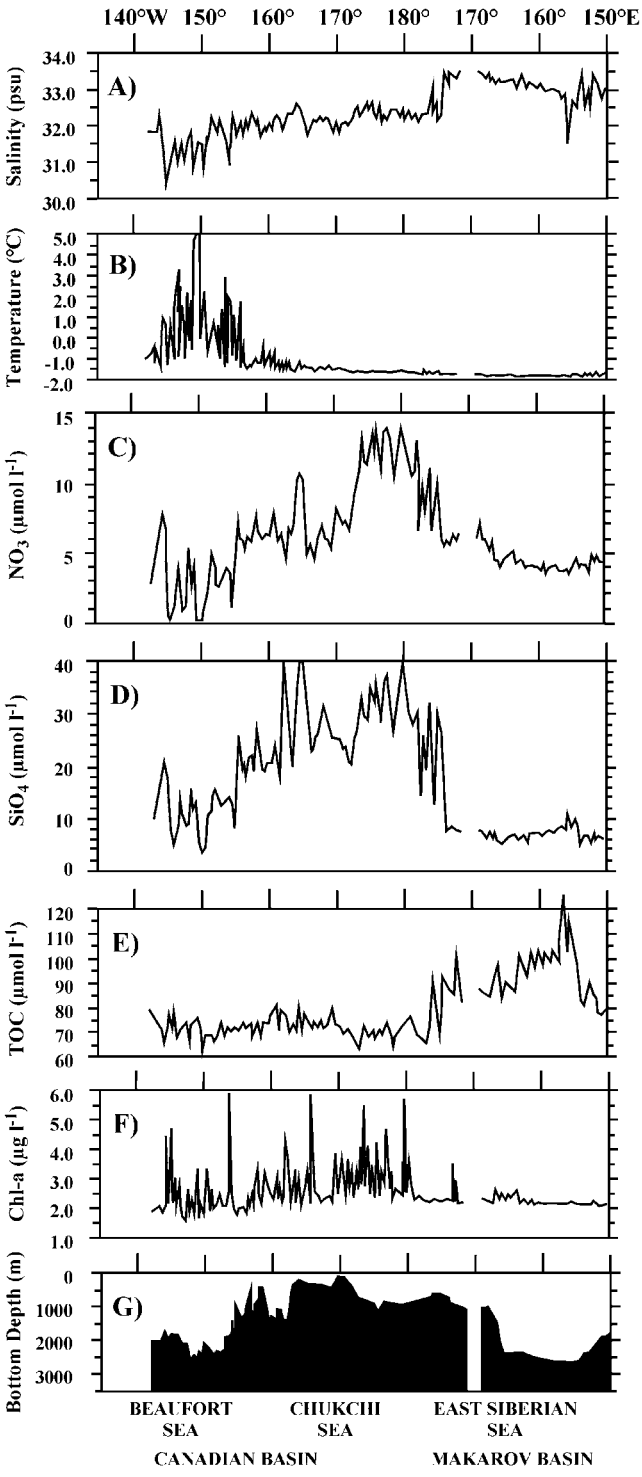


**Figure 3.** Fall distributions of Arctic (a) salinity, (b) temperature, (c) nitrate, (d) silicate, (e) DOC + POC, and (f) chlorophyll sampled by *Archerfish* at a nominal depth of 60 m during September 1997 along (g) the slope section shown in Figure 1 (Figures 3a, 3b, 3e, and 3g are redrawn from *Guay et al.* [1999]). These observations represent the positive, cyclonic phase of the AO with warmer temperatures and greater northward transport through Bering Strait.

0.5 ug chl $l^{-1}$ (10% diatoms; 5% prymnesiophytes; 85% microflagellates), 2125 umol DIC $kg^{-1}$, 0.5 umol C-copepods $kg^{-1}$, 2.0 umol C-protozoans $kg^{-1}$, a total of 60 umol DOC $kg^{-1}$, and 2.0 umol C-bacteria $kg^{-1}$ (Table 1). The boundary condition of ACW within shallow Bering Strait begins with this initial condition as well. At depths of >65 m, the initial and boundary conditions of Atlantic waters are 0.5–15.0 umol $NO_3$ $kg^{-1}$, 5.0–15.0 umol $SiO_4$ $kg^{-1}$, 0.1 umol $NH_4$ $kg^{-1}$, 0.2–0.0 ug chl $l^{-1}$ (10% diatoms; 5% prymnesiophytes; 85% microflagellates), 2125–2200 umol DIC $kg^{-1}$, 0.1–0.5 umol C-copepods $kg^{-1}$, 0.2–2.0 umol C-protozoans $kg^{-1}$, a total of 60 umol DOC $kg^{-1}$, and 0.8–2.0 umol C-bacteria $kg^{-1}$ (Table 3).

[17] Observed ice fields [*Chapman and Walsh*, 1993], net shortwave radiative fluxes [*Kistler et al.*, 2001], and a background $K_z$ are imposed over the spatial grid of the ecological models, extending at 9-km resolution from 170°E in the East Siberian Sea to 130°W in the Beaufort Sea and from Bering Strait to the 2000-m isobath of the Canadian Basin (Figure 1). It is nested within the larger spatial domain of the Pan-Arctic circulation model [*Maslowski and Lipscomb*, 2003] over all Arctic seas and basins at the same resolution of a 1/12° horizontal grid and a 45 layer vertical grid. The physical and plankton models have the same vertical resolution, which is highest near the surface, with 15 layers of minimal thickness of 5 m and maximal thickness of 20 m within the upper 200 m of the water column. The benthos model has one layer of a well mixed, 1-cm thickness, over which temperature impacts the rate of bioturbation. Details are provided in Appendix A.

[18] From prior runs, the physical model provides daily inputs of wind stress, salinity, temperature, and u, v to the ecological ones during August and September of the cyclonic and anticyclonic scenarios. Given the u, v fields, w in the plankton model is calculated from the equation of continuity for tracer transport as formulated in the Parallel Ocean Program [*Smith and Gent*, 2002]. We corrected for small differences (<= 0.3 Sv) between the inflow and outflow of water through the boundaries of the nested biological subdomain with a Lagrange multiplier technique [*Stoddard and Walsh*, 1986]. To evaluate the relative importance of these horizontal advective fields, September carbon budgets of each case are constructed from most terms of state equations (A1)–(A8) and (A12) for the different types of plankton, DOC, and DIC, given in Appendix A. Influxes from local rivers are presently ignored, since the DOC signature [*Amon and Benner*, 2003] of fresh, nutrient-poor "summer" ACW was smaller than that of AW during September 1997 (Figure 3e) in the Canadian Basin, while terrestrial loading of Russian rivers was mainly restricted to the Makarov Basin [*Guay et al.*, 1999].

## 3. Results

[19] The northward transports through Bering Strait of the coupled models at the end of July, August, and September were larger and warmer in 1989 than in 1980, with less amounts of snow and ice imposed at the surface of the water column (Figure 4). Indeed, northward (Figure 5a), not southward (Figure 5b), flow is simulated at a depth of ~30 m along the Russian coast on 30 September in the

**Table 1.** State Variables of Coupled Ecological Models of the Bering/Chukchi Seas

| Variable | Model |
|---|---|
| | *Plankton* |
| $P_d$ | Diatoms |
| $P_p$ | *Phaeocystis pouchetti* |
| $P_f$ | Microflagellates |
| B | Bacteria |
| $G_c$ | Copepods |
| $G_\mu$ | Protozoans |
| | *Nutrients* |
| $NO_3$ | Nitrate + nitrate |
| $NH_4$ | Ammonium |
| $SIO_4$ | Silicate |
| $DSIO_4$ | Interstitial silicate |
| | *Dissolved Carbon* |
| $DOC_1$ | Monomeric DOC |
| $DOC_2$ | Macromolecular DOC |
| DIC | Inorganic carbon |
| DS | Interstitial DIC |
| | *Detritus* |
| $Z_c$ | Settling siliceous fecal pellets |
| $Z_\mu$ | Settling nonsiliceous fecal pellets |
| $S_p$ | Nonsiliceous sediment particulate carbon |
| $S_{ps}$ | Siliceous sediment particulate carbon |

anticyclonic case of 1980, with reversal of the usual northward flow along the Alaskan coast as well. At the same depth, model temperatures of ACW, with salinities of <32 on this day in 1989 (Figure 6b), are warmer than in 1980 (Figure 7a), with a maximum of 6.3°C (Figure 7b), similar to that observed by the *Archerfish* within the Beaufort Sea during another cyclonic period of September 1997 (Figure 3b).

[20] Along the 50-m isobath of the south central Chukchi Sea, the stronger northwestward flows (Figure 5b) of high salinity (Figure 6b), low temperature (Figure 7b) AW advect 4–6 umol $NO_3$ $kg^{-1}$ and 15–20 umol $SiO_4$ $kg^{-1}$at a depth of ~30 m about 130 km farther toward Wrangel Island in September 1989 (Figures 8b and 9b) than in the same month of 1980 (Figures 8a and 9a). Similarly, the near-bottom nitrate and silicate contents of AW on the 40-m isobath of the *Polar Sea*/*Louis St-Laurent* section at 70°N, 168°45′W (shown by solid circles in Figure 1) were >15 umol NO3 $kg^{-1}$ and >50 umol $SiO_4$ $kg^{-1}$ [*Wheeler et al.*, 1997] during the very large northward transport of the1994 cyclonic period (Figure 2b). At this same location in September 1990, under annual northward transport of 73% that of 1994 [*Roach et al.*, 1995], <2 umol $NO_3$ $kg^{-1}$ and <10 umol $SiO_4$ $kg^{-1}$ were instead found here within AW [*Cooper et al.*, 1997]. In August 1988, at 55% of the 1994 annual transport, these near-bottom AW stocks of <2 umol $NO_3$ $kg^{-1}$ and <10 umol $SiO_4$ $kg^{-1}$ were then observed south of 68°30′N [*Walsh et al.*, 1989].

[21] In the northwestern Chukchi Sea, however, within deeper regions of >60% surface ice cover, more nitrate and silicate are left unutilized at a depth of 30 m on 30 September 1980 (Figures 8a and 9a), despite weaker northward advection of Pacific nutrients (Figure 5a), as a result of greater light limitation (Figure 10a). The depth integral of photosynthesis covaried with the ice cover, moreover, such that the model's fixation of ~200 mg C $m^{-2}$ $day^{-1}$ in mid-September 1980 and 1989 (Figures 11a and 11b) was roughly associated with ~60% ice cover (Figures 10a and 10b). Higher primary production of >1000 mg C $m^{-2}$ $day^{-1}$ on 15 September is simulated under <20% ice cover during both scenarios of the coupled models within regions of little ice, such that the spatial extent rather than the depth integral of algal carbon synthesis changes from year to year. Over the model grid, a 50% increase of total carbon fixation occurs during 15 August to 15 September 1989, compared with the same period in 1980. On a unit basis, similar ranges of 100–2570 mg C $m^{-2}$ $day^{-1}$ of net production were measured under 55–80% ice cover during August 1994 [*Gosselin et al.*, 1997] and 102–486 mg C $m^{-2}$ $day^{-1}$ under 20–40% ice cover in August 1993 [*Cota et al.*, 1996].

[22] Simulated surface chlorophyll stocks of 3–5 ug chl $l^{-1}$ (Figures 12a and 12b) of mainly diatoms (Figures 13a and 13b) over most of the Chukchi/Beaufort shelves during 30 September 1980 and 1989 are similar to those observed on the inner shelf in August 1988 [*Walsh et al.*, 1989]. Subsurface maxima of 3–5 ug chl $l^{-1}$ were also found at depths of 30–40 m, above the upper slope (~350 m isobath) [*Macdonald et al.*, 1995] and outer shelf (~60 m isobath) [*Cota et al.*, 1996] of the Chukchi Sea, during ice-breaker cruises in August and September 1993 (Figure 1). Finally, total phytoplankton stocks of 3–5 ug chl $l^{-1}$ were measured at a depth of 60 m (Figure 3f) along the *Archerfish* transect [*Guay et al.*, 1999] above the midslope region (500–1000 m isobaths) of the Chukchi Sea (Figure 3g) in September 1997.

[23] In terms of dominant functional groups, *Phaeocystis* won (Figures 13a and 13b) in regions of <0.5 ug chl $l^{-1}$ (Figures 12a and 12b) and >80% ice cover (Figures 10a and 10b), particularly during the poorer light regime of September 1980. Although *Phaeocystis* grew better at low light intensities (see Appendix A), their realized growth rates in these regions were very low (<0.01 $day^{-1}$), and the higher prymnesiophyte biomass of the models was due primarily to both selective grazing of diatoms by relatively abundant copepods and greater initial stocks of *Phaeocystis* than microflagellates in Anadyr Water.

[24] Biomarkers suggested a dominance of diatoms within surface waters and sediments of the Chukchi shelf, with usually a minor contribution from *Phaeocystis*, during August 1994 and 2000 [*Belicka et al.*, 2002]. However, at a total surface stock of 0.5 ug chl $l^{-1}$, fatty acids then indicated that *Phaeocystis* dominated the phytoplankton, as in the model. Similar dominance of *Phaeocystis* was simulated and observed in deeper regions of the Ross Sea [*Arrigo et al.*, 2003]. Finally, microflagellates were the dominant group in slope and basin regions of the model, where the different size classes of autotrophic flagellates constituted ~74% of the carbon biomass in August 1994 [*Booth and Horner*, 1997].

[25] The increasing depth in the water column stocks of subsurface maxima of 3–5 ug chl $l^{-1}$, from inner shelf to slope [*Walsh et al.*, 1989; *Cota et al.*, 1996; *Macdonald et al.*, 1995; *Guay et al.*, 1999], and the sediment biomarkers [*Belicka et al.*, 2002] both suggest fallout of dominant populations of larger diatoms [*Booth and Horner*, 1997] in the Chukchi Sea during August 1988, 1993, 1994, and 2000. After settling to a depth of 30 m, the spatial extent of

**Table 2.** Model Parameters[a]

| Variable | Amount | Definition |
|---|---|---|
| $c_i$ | [0.70, 0.70, 0.76] $e^{.0633T}$ | Maximum growth rate as a function of temperature, T, $day^{-1}$ |
| $g_i$ | – | Algal growth as a function of light and nutrients, $day^{-1}$ |
| $g_{i,NO_3}$ | – | Algal uptake rate, nitrate, $day^{-1}$ |
| $g_{i,NH_4}$ | – | Algal uptake rate, ammonium, $day^{-1}$ |
| $g_{i,SIO_4}$ | – | Algal uptake rate, silicate, $day^{-1}$ |
| $\varepsilon_i$ | [0.10, 0.05, 0.05] | Algal respiration rate, percent of $g_i$ |
| $\psi_i$ | [0.04, 0.04, 0.40] | Algal excretion of $DOC_1$, percent of $g_i$ |
| L(t, z) | – | Photosynthetic active radiation in the water column, W $m^{-2}$ |
| $L_{is}$ | [45, 35, 25] | Saturation (optimal) light intensity for growth, W $m^{-2}$ |
| $I_m$ | – | Maximum noon radiation, W $m^{-2}$ |
| $I_p$ | – | Daily mean PAR, W $m^{-2}$ |
| $R_b$ | 0.5 | Fraction of surface PAR in the blue-green wavelengths |
| $t_s$ | – | Time since sunrise, hours |
| $\Delta$ | – | Photoperiod, hours |
| $\pi$ | 3.14... | |
| $c_b$ | $0.008e^{0.092T}$ | Maximum bacterial growth rate as a function of T, $hours^{-1}$ |
| m | 0.002 + 0.005T | Bacterial mortality rate as a function of temperature, $hours^{-1}$ |
| $g_3$ | – | Bacterial uptake rate of $DOC_1$, $day^{-1}$ |
| $g_4$ | – | Bacterial uptake rate of $DOC_2$, $day^{-1}$ |
| $\beta$ | $0.5(g_3 + g_4)$ | Bacterial respiration, $day^{-1}$ |
| $\eta_i$ | [0.0, 0.0, 0.0] | Algal lysis to $DOC_2$, percent algal biomass per day |
| $\eta_{c,\mu}$ | [0.0, 0.0] | Fecal pellet lysis, percent fecal pellet biomass per day |
| $\gamma_d$ | 0.20 | Grazing loss of diatoms, percent copepod body carbon per day |
| $\zeta$ | 0.1 | Protozoan grazing coefficient, umole C $kg^{-1}$ $day^{-1}$ |
| $\gamma_\mu$ | $\zeta(P_f + P_p)$ | Protozoan daily ration, % protozoan body carbon per day |
| $\gamma_f G_\mu$ | – | Microflagellate grazing by protozoans, umole C $kg^{-1}$ $day^{-1}$ |
| $\gamma_p G_\mu$ | – | *Phaeocystis* grazing by protozoans, umole C $kg^{-1}$ $day^{-1}$ |
| $P_{ps}$ | $0.9P_p$ | Single-cell *Phaeocystis* concentration, umole C $kg^{-1}$ |
| $w_d$ | $0.025P_d^2$ | Diatom settling velocity, m $day^{-1}$. $P_d$ in ug chl $l^{-1}$ |
| $w_p$ | $0.025P_p^2$ | *Phaeocystis* settling velocity, m $day^{-1}$. $P_p$ in ug chl $l^{-1}$ |
| $w_f$ | 0.5 | Microflagellate settling velocity, m $day^{-1}$ |
| $w_{zd}$ | 100.0 | Settling velocity, siliceous fecal pellets, m $day^{-1}$ |
| $w_{zf}$ | 30.0 | Settling velocity, nonsiliceous fecal pellets, m $day^{-1}$ |
| $\alpha_{c,\mu,b}$ | [0.325, 0.60, 0.20] | POC respired by copepods, protozoans, and carnivores, % |
| $\varphi_{c,\mu,b}$ | [0.50, 0.0, 0.50] | $DOC_2$ from sloppy copepods, protozoans, and carnivores, % |
| $[1 - \alpha_{c,\mu,b} - \varphi_{c,\mu,b}]$ | – | Fecal pellet production from herbivores and carnivores |
| $Grmin_i$ | [0.05, 0.05, 0.05] | Grazing threshold, ug chl $l^{-1}$ |
| $Grlayer_{c,\mu}$ | [200, 100] | Maximum extent of copepod/protozoan grazers, m |
| $k_{iNO_3}$ | [0.9, 0.9, 0.9] | Half-saturation constant for nitrate uptake, umole N $kg^{-1}$ |
| $k_{iNH_4}$ | [0.2, 0.2, 0.2] | Half-saturation constant for ammonium uptake, umole N $kg^{-1}$ |
| $k_{iSIO_4}$ | [1.15, 0.0, 0.0] | Half-saturation constant for silicate uptake, umole Si $kg^{-1}$ |
| $k_{DOC}$ | 0.83 | Half-saturation constant for $DOC_{1,2}$ uptake, umole C $kg^{-1}$ |
| $k_{NIT}$ | 0.10 | Half-saturation constant for nitrification, umole N $kg^{-1}$ |
| $k_b$(w, i, s) | [0.0438, 2, 15] | Attenuation of blue-green light, $m^{-1}$, in seawater, ice, snow |
| $k_r$(w, i, s) | [0.40, 4.0, 35] | Attenuation of red light, $m^{-1}$, in seawater, ice, and snow, |
| $k_c$ | – | Attenuation coefficient of chlorophyll, $m^{-1}$ |
| $k_m$ | – | Attenuation coefficient of CDOC, $m^{-1}$ |
| k(a) | 0.38 | Attenuation coefficient of ice algae, $m^{-1}$ |
| $k_i$ | [0.024, 0.048, 0.012] | Specific algal attenuation coefficient, $m^2$ (mg chl)$^{-1}$ |
| $k_y$ | $47.0 \times 10^{-6}$ | Specific CDOC attenuation coefficient, $m^2$(mg DOC)$^{-1}$ |
| z(i, s, a) | [2.0, 0.1, 0.01] | Thickness of ice, snow, and ice algae layers, m |
| $X_1$ | – | Nitrification rate, umoles N $kg^{-1}$ $s^{-1}$ |
| $X_2$ | 0.20 | Photolytic loss of $DOC_2$ to $DOC_1$, umole DOC $kg^{-1}$ $hour^{-1}$ |
| $\lambda$ | 5.0 | Degradation rate sediment particulate organic carbon, $day^{-1}$ |
| $K_b$ | $3.5 \times 10^{-4}$ $e^{0.092Tb}$ | Bioturbation coefficient and bottom temperature $T_b$, $m^2$ $s^{-1}$ |
| $K_m$ | $3.5 \times 10^{-10}$ | Porewater diffusion coefficient, $m^2$ $s^{-1}$ |
| $K_h$ | $1.0 \times 10^{-4}$ | Water column eddy diffusivity, $m^2$ $s^{-1}$ |
| $(C/N)_r$ | (100/15) | Redfield molar C/N ratio in all organic matter except bacteria |
| $(C/Si)_r$ | (100/15) | Redfield molar C/Si ratio of diatoms and siliceous fecal pellets |
| $(C/N)_b$ | (100/20) | Molar C/N ratio of bacteria |
| $(C/CHL)_i$ | [45, 50, 125] | Particulate organic carbon/chlorophyll ratio, ug/ug |

[a]Subscript i is d, f, p for diatoms, microflagellates, and *Phaeocystis*.

simulated near-bottom stocks of >10 ug chl $l^{-1}$ near Alaska was larger on 30 September 1980 (Figure 14a) than during 1989 (Figure 14b), as a consequence of the southward flows along the coast of the anticyclonic regime (Figure 5a).

[26] During the weak annual northward transport of 1987 (Figure 2b), southeastward displacement of AW towards Kotzebue Sound led to near-bottom stocks of >40 chl $l^{-1}$ within the eastern Chukchi Sea in August [*Springer and McRoy*, 1993] as well and actual flow reversals within Bering Strait during September [*Coachman*, 1993]. Greater fallout of plankton debris to the model's sea bottom also occurred in this region of the model during 30 September 1980 (Figure 15a), but because of the more extensive primary production in 1989 (Figure 11b), the overall mean

**Table 3.** Pacific and Atlantic Summer Initial and Boundary Conditions of Nutrients, Dissolved Inorganic Carbon, Total Phytoplankton Biomass, Copepods, Protozoans, Dissolved Organic Carbon, and Bacterioplankton[a]

| Depth | Nitrate | Ammonium | Silicate | DIC | Algae | Copepods | Protozoans | DOC | Bacteria |
|---|---|---|---|---|---|---|---|---|---|
| | | | | *Anadyr Water* | | | | | |
| 0 | 5 | 0.5 | 20 | 2050 | 0.5 | 1 | 1 | 90 | 1 |
| 30 | 10 | 0.5 | 25 | 2050 | 0.5 | 1 | 1 | 90 | 1 |
| 65 | 15 | 0.5 | 30 | 2050 | 0.5 | 1 | 1 | 90 | 1 |
| 220 | – | – | – | – | – | – | – | – | – |
| | | | | *Alaska Coastal Water/Canadian Basin* | | | | | |
| 0 | 0.5 | 0.5 | 5 | 2125 | 0.5 | 0.5 | 2 | 60 | 2 |
| 30 | 0.5 | 0.5 | 5 | 2125 | 0.5 | 0.5 | 2 | 60 | 2 |
| 65 | 0.5 | 0.5 | 5 | 2125 | 0.5 | 0.5 | 2 | 60 | 2 |
| 220 | 9.0 | 0.1 | 6 | 2150 | 0.2 | 0.5 | 2 | 60 | 0.8 |
| >220 | 15.0 | 0.1 | 15 | 2200 | 0.0 | 0.1 | 0.2 | 60 | 0.8 |

[a]Anadyr Water in Bering Strait and over depths <65 m contains 85% diatoms, 10% *Phaeocystis*, and 5% microflagellates, whereas the model's phytoplankton community is 85% microflagellates, 10% diatoms, and 5% *Phaeocystis* within Alaska Coastal Water and deeper shelf/slope regions. All units are umol $kg^{-1}$ of N, Si, and C, except ug chl $l^{-1}$.

POC flux into the sediments increased by an increment of 33% in the 1989 case (Figure 15b).

[27] The amount of sediment debris also increased within the south central part of the Chukchi Sea during the cyclonic scenario of 1989 (Figure 15b), like the northwestward dispersion (Figure 5a) then of nutrient supplies (Figures 8b and 9b) and carbon fixation (Figure 11b) towards Wrangel Island. During the anticyclonic period of 1987, high sediment oxygen uptake rates were instead found just north of Bering Strait [*Grebmeier*, 1993]. In contrast, remineralization of organic matter appeared to similarly occur near the shelf break during the other 1994 cyclonic regime, based upon low near-bottom oxygen concentrations found on the ~110-m isobath [*Swift et al.*, 1997].

[28] The simulated maxima of ammonium pools, regenerated at the 30-m (Figures 16a and 16b) and 60-m isobaths, were 2–4 umol $NH_4$ $kg^{-1}$ on 30 September 1980 and 1989, the same as those measured near the bottom of the Chukchi Sea during August 1987 [*Walsh et al.*, 1989] and September 1990 [*Cooper et al.*, 1997]. Like the northwestward translation of new nitrogen supply and total primary production in 1989 (Figures 8b and 11b), recycled nitrogen of >2.5 umol $NH_4$ $kg^{-1}$ was more extensive around Wrangel Island during 1989 (Figure 16b), supporting suggestions of changing loci of bottom metabolism, inferred from the 1987 and 1994 oxygen data [*Grebmeier*, 1993; *Swift et al.*, 1997].

[29] Under stronger poleward flows along the Alaskan coast of the model's cyclonic regime (Figure 5b), the ACW boundary condition of 60 umol DOC $kg^{-1}$ (Table 1) propagated northward on the Chukchi shelf to Cape Lisburne at a depth of 30 m by 30 September 1989 (Figure 17b). However, since the boundary condition of the Canadian basin was also 60 umol DOC $kg^{-1}$ above bottom depths of >65 m, larger DOC stocks at the shelf edge must instead represent export of some of the primary production residues of the fall autotrophic shelf ecosystem. Indeed, at a depth of 60 m, the sum of the model's separate pools of ~65 umol DOC $kg^{-1}$ (Figure 18b) and 1 ug chl $l^{-1}$ (Figure 19b), or ~4 umol POC $kg^{-1}$, above the 2000-m isobath at 150°W of the Beaufort Sea on 30 September 1989 match the total of ~70 umol TOC $kg^{-1}$ sampled there by *Archerfish* in September 1997 (Figure 3e). Farther west at 173°W, ~70 umol TOC $kg^{-1}$ was also found at a depth of 60m above the 2000-m isobath of the Chukchi Sea in August 1994 [*Wheeler et al.*, 1997] but the POC component may be larger there (Figure 3f).

[30] Like the zooplankton populations of the southeastern Bering Sea, where the Hokkaido study (Figure 2d) found that their biomass of the 1972–1979 anticyclonic period was half that of the cyclonic regime during 1964–1971 [*Sugimoto and Tadokoro*, 1997], the model's mean secondary production of fecal pellets of copepods and protozoans during August and September was 19.6 mg C $m^{-2}$ $day^{-1}$ in 1980, compared with 28.3 mg C $m^{-2}$ $day^{-1}$ in 1989. The grazing stresses exerted by these copepods and protozoans were then at most ~50% of the model's daily net photosynthesis of 115–184 mg C $m^{-2}$ $day^{-1}$ on the outer shelf.

[31] Low ingestion rates imply small export of settling POC from a depth of 60 m on the outer Chukchi/Beaufort shelves (Figures 19a and 19b), where the diatoms and microflagellates were now the dominant functional groups

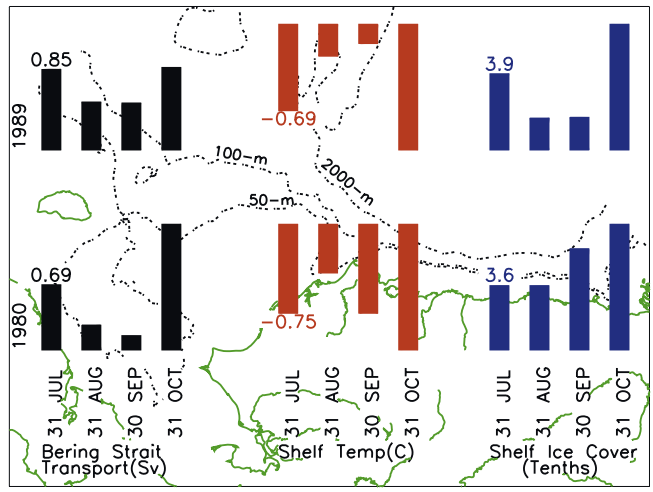


**Figure 4.** The northward transport (Sv) through Bering Strait in relation to the mean shelf (<100 m) temperature (°C) and ice cover (%) over the Chukchi/Beaufort shelves on 31 July, 31 August, 30 September, and 31 October during 1980 and 1989.

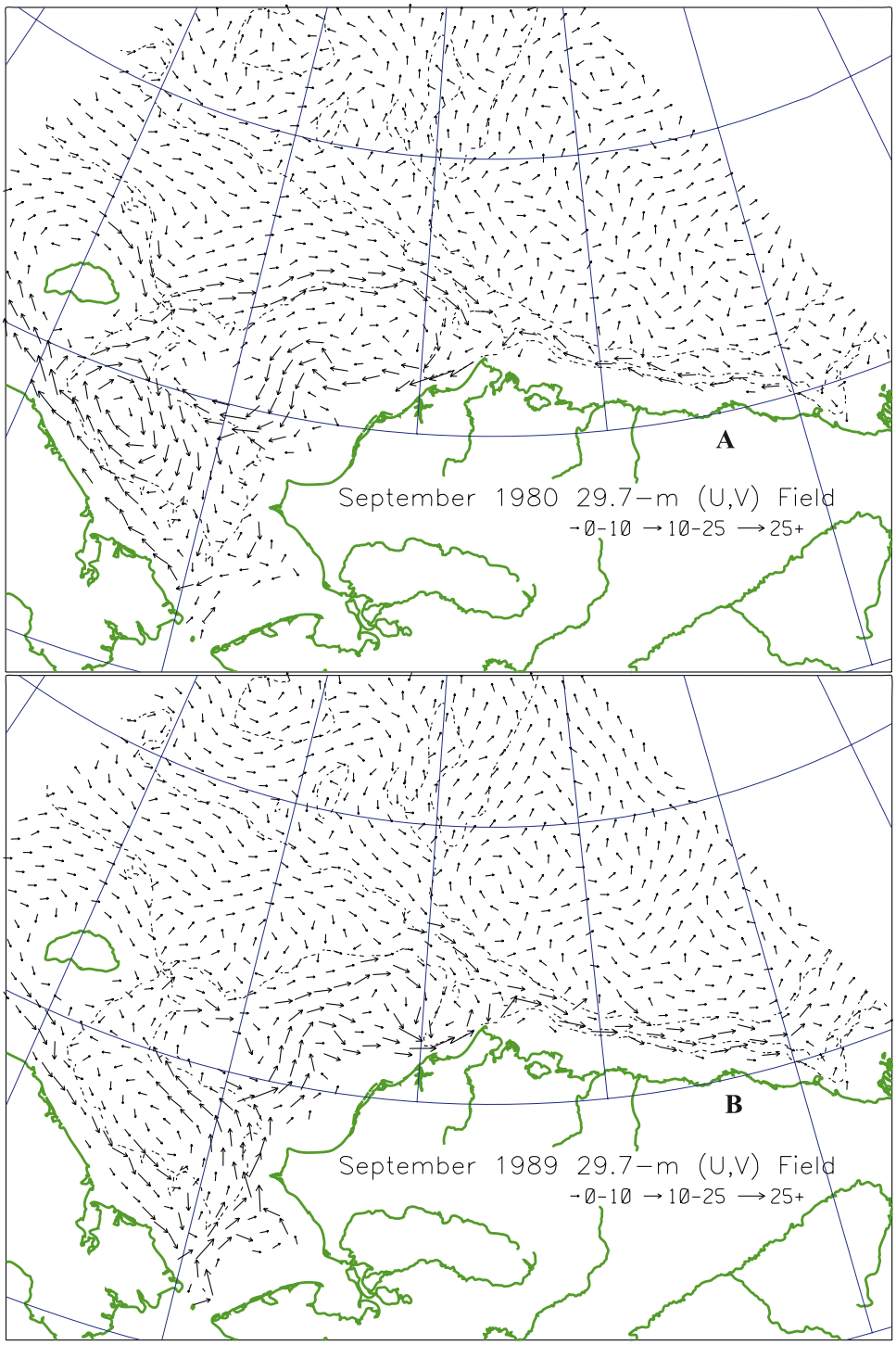


**Figure 5.** The horizontal currents (cm $s^{-1}$) at a depth of ~30 m on 30 September (a) 1980 and (b) 1989.

near the bottom of the euphotic zone in both scenarios (Figure 20a and 20b). However, zooplankton debris settles much faster than that of phytoplankton in our model (Table 2). Of the POC reaching these sediments of the model, phytoplankton debris amounted to only ~55% each year, with the rest contributed by fecal pellets of the herbivores and carnivores. Since cholesterol is one of the most abundant sterols in the Chukchi shelf sediments [*Belicka et al.*, 2002] and can be a zooplankton biomarker, their significant contribution to particle export here may be correctly identified in the model results.

[32] A predicted lateral export of particulate matter from these Arctic shelves to the basins during late summer and early fall suggests that they should then, at least, be a sink of atmospheric $CO_2$. Indeed, most of the simulated Chukchi shelf was a weak September sink of atmospheric $CO_2$ in both the 1980 and 1989 cases (Figures 21a and 21b), while the Beaufort shelf was a source in the former and a sink in

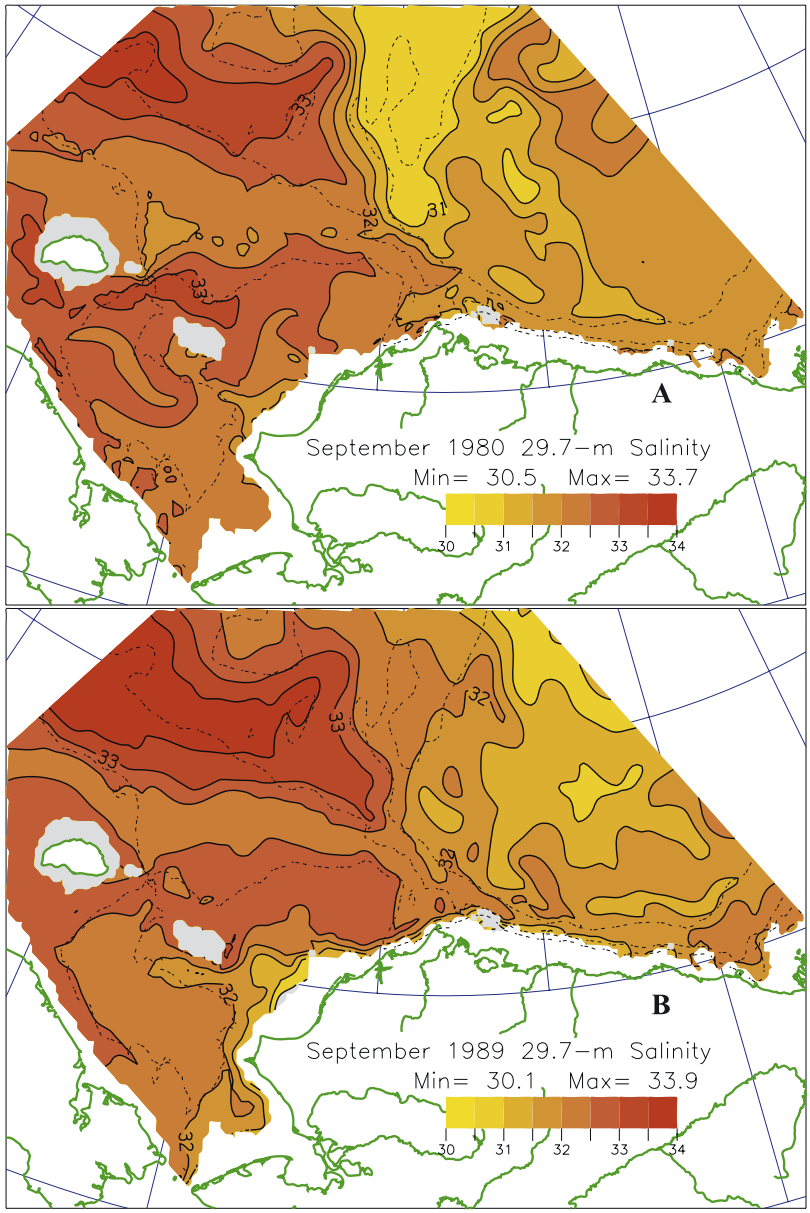


**Figure 6.** The fields of salinity at a depth of ~30 m on 30 September (a) 1980 and (b) 1989.

the latter. A surface seawater $pCO_2$ of 248 uatm was simulated near 155°W on the Beaufort shelf on 30 September 1989 (Figure 21b), where ~250 uatm was measured during September 2000 [*Murata and Takizawa*, 2003]. These surface sea water values are lower than the atmospheric $pCO_2$ amounts of 362 uatm found above Barrow, Alaska and the Chukchi Sea in 2001 [*Murata and Takizawa*, 2003] and still smaller than the 315 uatm sampled earlier above the Bering Sea in 1968 [*Kelley and Hood*, 1971].

[33] At the same location, the model's estimate of $pCO_2$ was 375 uatm on 30 September 1980 (Figure 21a), however, when outgassing would have instead prevailed, as in slope waters of the Canadian Basin during both years. We attribute these interannual differences in DIC stocks and thus $pCO_2$ of surface seawater on the Beaufort shelf to a combination of increased eastward advection (Figure 5) of well-lit (Figure 10), nutrient-impoverished (Figures 8–9), $CO_2$-depleted, plankton-rich residues (Figures 12, 14, and 19) and prior, upstream primary production (Figure 11) during the cyclonic phase of warmer temperatures (Figure 7), i.e., when the solubility of $CO_2$ gas would be less, and thus the $pCO_2$ of surface waters should be larger, not smaller as observed [*Murata and Takizawa*, 2003]. The shelf-wide mean contribution of advection to these changes is discussed in the last section of the paper.

[34] These simulations do not allow a complete analysis of shelf export, however, since we did not attempt to incorporate the nitrate/silicate contents of the Anadyr plume beyond the shelf break as part of the initial conditions, and we considered only the August and September time frame. Seaward propagation over time of unknown winter conditions at Bering Strait thus remains unresolved, such that

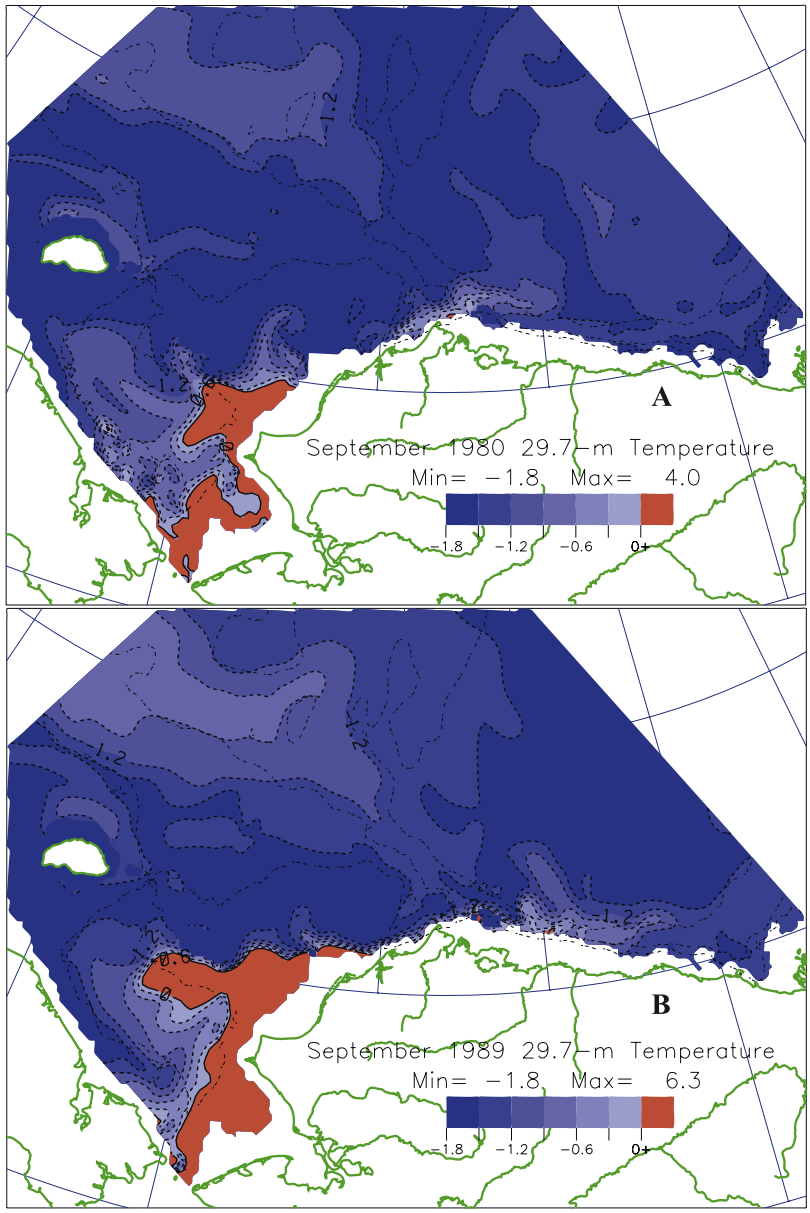


**Figure 7.** The fields of temperature (°C) at a depth of ~30 m on 30 September (a) 1980 and (b) 1989.

total amount of export of all dissolved materials is an unanswered question. The present results of these models on 30 September (Figures 22a and 22b) do not replicate the export of unutilized, relict winter stocks of silicate and nitrate, found in AW at a depth of 60 m along the slope in 1997 (Figures 3c and 3d).

[35] Above the 2000-m isobath, the isopleth of ~7 umol $NO_3$ $kg^{-1}$ in the cyclonic case of September 1989 extended east past 150°W into the Beaufort Sea (Figure 22b), as measured (Figure 3c) in ACW (Figures 3a and 3b) during September 1997 but not simulated in the anticyclonic scenario of 1980 (Figure 22a). Farther west past 175°W in the Chukchi Sea, ~12 umol NO3 $kg^{-1}$ was simulated during September 1989 above the ~100-m isobath (Figure 22b) but observed at the ~1000-m isobath in 1997 (Figures 3c and 3g). Since this region of the Chukchi Sea is usually light-limited (Figure 10b), the fidelity of the present model was otherwise excellent, until future global warming melts more of the ice pack!

## 4. Discussion

[36] Any long-term change in prey availability to whales [*Schell*, 2000] may just reflect a spatial dislocation of the plankton transfer of nutrient supplies up the food web during decadal shifts of flow fields, from anticyclonic regimes to cyclonic ones, associated perhaps with a more positive AO since 1900 [*Kerr*, 1999]. To evaluate the importance of advection within the Chukchi/Beaufort Seas, we constructed carbon budgets (Figures 23a and 23b) of each term of the state equations in Appendix A for the time-dependent behavior of the model's variables of living plankton POC (the sums of all algal groups and of the bacteria), the zooplankton pellets as detrital POC in the

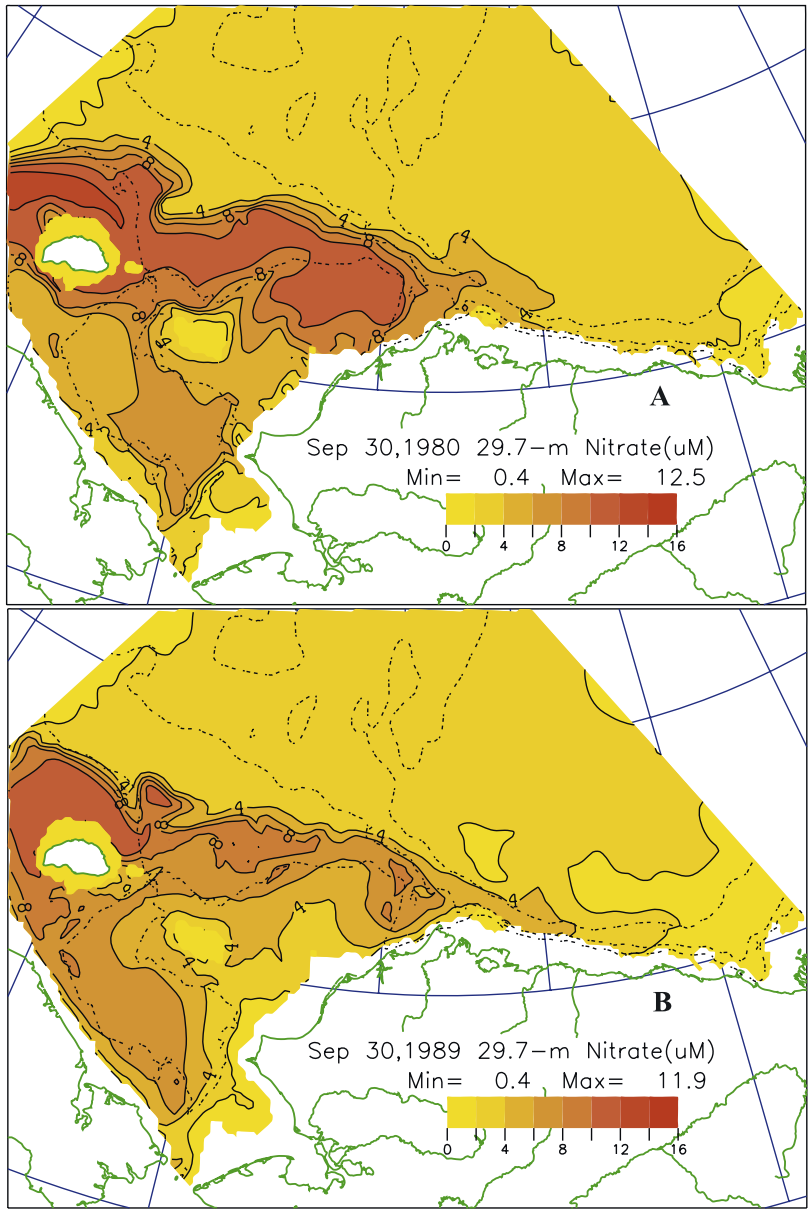


**Figure 8.** The fields of nitrate (umol $NO_3$ $kg^{-1}$) at a depth of ~30 m on 30 September (a) 1980 and (b) 1989.

water column, the sum of monomeric and macromolecular DOC, and the DIC.

[37] Averaged over the Chukchi/Beaufort shelves of <220 m depth during September 1980 and 1989, for example, the model results suggest that both regions were an atmospheric $CO_2$ sink of 95.9–145.9 mg C $m^{-2}$ $day^{-1}$ (Figures 23a and 23b). The modeled system is not in steady state over this time frame; 34% of both September 1980 and 1989 production went to an increase in standing stocks of the phytoplankton functional groups and the remaining 66% to other compartments of the system. Consequently, in the two cases of the model, their September water column inventory of DIC increased at rates of 8.0–145.9 mg DIC $m^{-2}$ $day^{-1}$. Of these increases, only 3.8–9.5%, or a mean of 6.7% of the September DIC increment, were attributed to advective losses or gains. Note that the increased biological draw down of $CO_2$ during alleviation of light limitation within the stronger flow regime of less ice cover during 1989 led to a mean September net production of 345.6 mg C $m^{-2}$ $day^{-1}$ in 1889, compared with 183.3 mg C $m^{-2}$ $day^{-1}$ in 1980 (Figures 23a and 23b).

[38] During 1980, 48% of the primary production was consumed by herbivores, with 11% and 7% lost to DOC and the sediments respectively. In 1989, 46% was harvested by herbivores with 15% and 5% directed to DOC and the sediments. The greater relative DOC yield in 1989 was due to higher prymnesiophyte primary production and their greater excretion rates, in comparison to those of the diatoms or microflagellates (Table 2). The increase of DOC excretion during 1989 fueled a corresponding increase of 16% in heterotrophic production of the bacterioplankton that year. Of the bacterial secondary production, 92% and

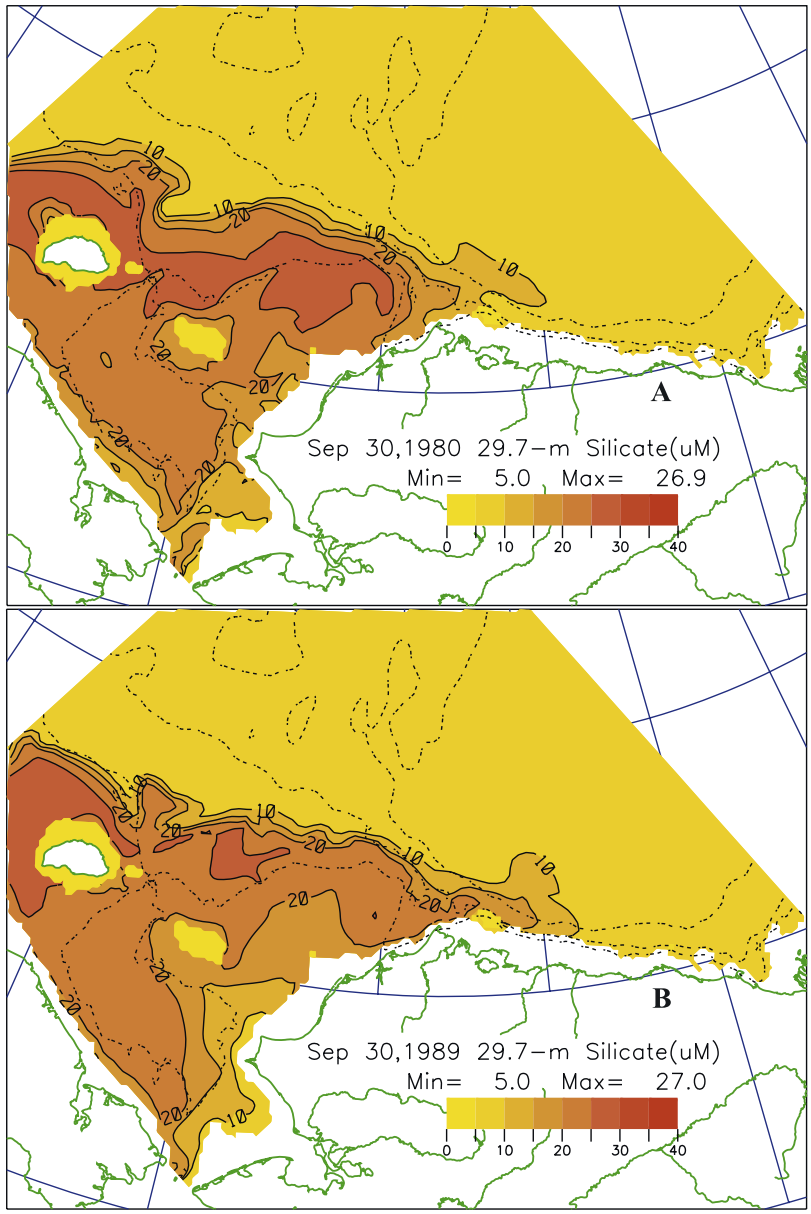


**Figure 9.** The fields of silicate (umol $SiO_4$ $kg^{-1}$) at a depth of ~30 m on 30 September (a) 1980 and (b) 1989.

90% was respired during 1980 and 1989, respectively, with about 25% of their carbon increment of secondary production taken by predators of the microbial web.

[39] Only the long-lived particles of ungrazed phytoplankton, with relatively low respiration and consumption losses, remained within the water column for a sufficient time to experience significant transport, such that a mean 7.5% of their net September daily POC increment of all stocks was effected by water movement in 1980 and 1989, compared with 4.3% for the fast settling fecal pellets and 1.7% for the bacterioplankton (Figures 23a and 23b). Food web changes, rather than advective ones, may thus have greater consequences in future Arctic responses to global climate oscillations.

[40] With respect to the grazers of similar and larger particle size, about 48% and 51% of the combined herbivore grazing stress was respired to DIC, with 30% and 33% converted to particulate detritus in 1980 and 1989, respectively. The relatively higher release of DOC from "sloppy" grazers in 1980, 22% versus 16%, was due to the higher fraction of copepod versus protozoan grazing stresses in 1980. The cycling of carbon by carnivores was as prescribed: 50% of their consumption returned as DOC, 30% became fecal pellets, and 20% was respired.

[41] We are pleased with most of the results of our coupled models that match prior observations of phytoplankton biomass and species composition, nutrient utilization and regeneration, and shelf export of DOC and POC, suggesting that years of cyclonic flow regimes led to a twofold areal increase of fall primary and secondary production, which was evidently not stored in the shelf sediments (Figures 23a and 23b). The sediment and DOC pools of carbon experienced a net loss for the month of September in both 1980 and 1989, while the detritus and

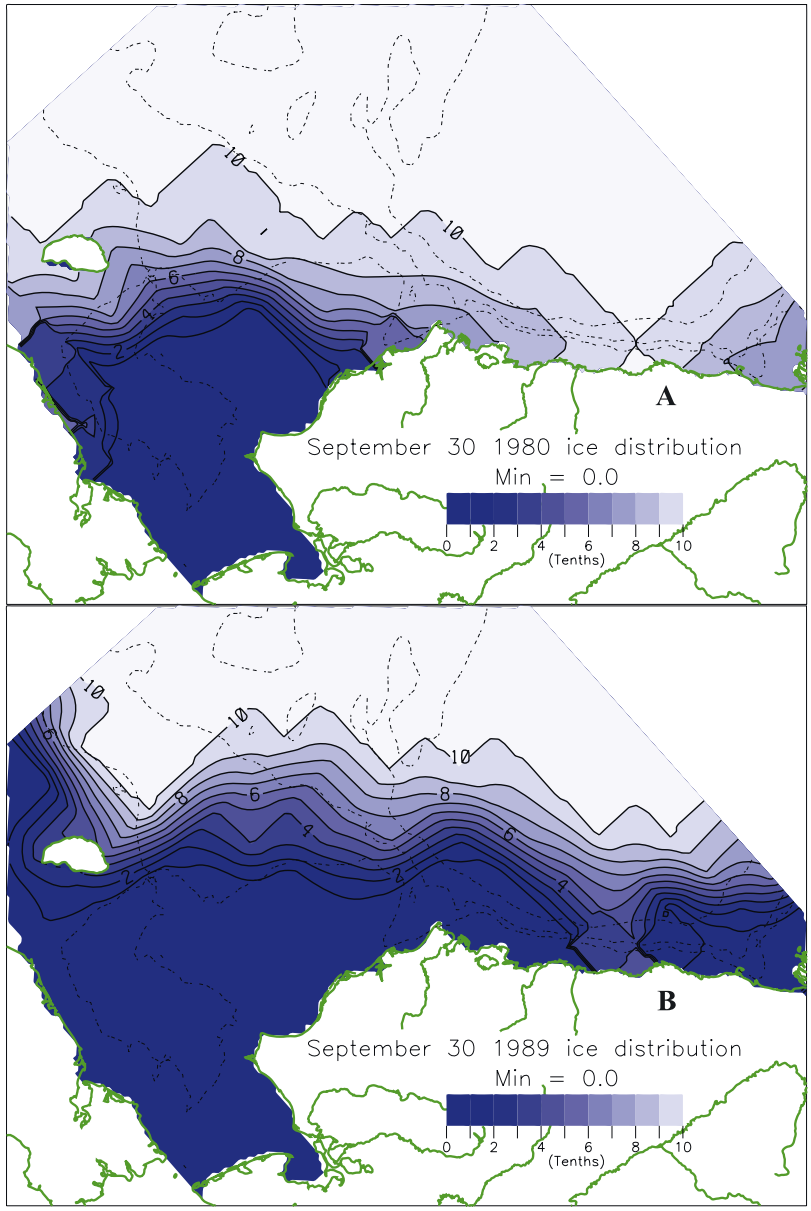


**Figure 10.** The imposed surface ice cover (%) at a the end of September (a) 1980 and (b) 1989.

DIC pools gained. The 52% increment of $CO_2$ influx to the water column from air-sea exchange in 1989 was a consequence of the higher net autotrophic production, since the solubility pump of warmer temperatures in 1989 actually retarded the storage of $CO_2$ gas [*Peng et al.*, 1987]. The greater biological uptake and invasion of $CO_2$ was offset by the higher total respiration rates of the sediment and water column biota, however, such that a smaller rate of increase of DIC stocks occurred in September 1989 than during the same month of 1980.

[42] Overall, 300 mg C $m^{-2}$ $day^{-1}$ of organic carbon was lost from the Chukchi and Beaufort shelves in September 1980, with an increase to about 1800 mg C $m^{-2}$ $day^{-1}$ during the same month of 1989. In both cases, this export represented a very small fraction of the initial pool of organic carbon. Moreover, the accumulation of fall POC in the shelf water column and the draw-down of DOC may most likely be due to deficiencies in modeling the exchange of POC and DOC across the sediment-water interface, a problem which was exacerbated by the poor resolution of the model in the vertical coordinate. Yet the future impact of offshore advection of settling shelf export from well-lit, ice-free regions to the south of the Canadian Basin may depend more upon how the unutilized winter supply of Pacific nutrients will be removed by which groups of phytoplankton at the Basin borders.

[43] A PN/chl (umol/ug) ratio of 0.6 [*Walsh et al.*, 1978] and a PN/PSI (umol/umol) ratio of 1.0 [*Brzezinski*, 1985] for diatom blooms suggest that the observed fall export of 5–6 ug chl $l^{-1}$ within AW at 60-m depth near 173°W (Figure 3f) is equivalent to a net removal in particulate form of 3–4 umol $kg^{-1}$ of both dissolved nitrate and silicate. The model results suggested a similar amount of 4–5 ug chl $l^{-1}$ near 173°W, at a depth of 60 m on the outer shelf (Figure 19b), where diatoms were dominant (Figure 20b). Such inferred nutrient stock reductions are consistent with a

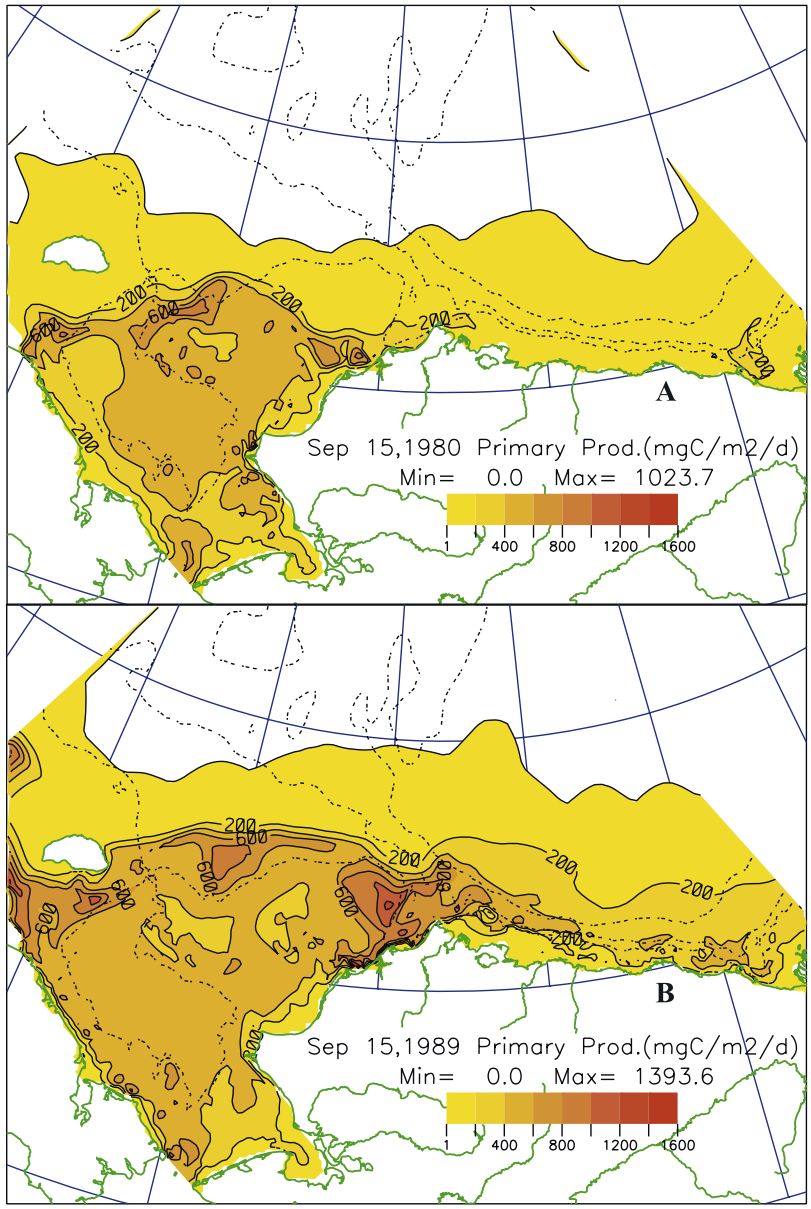


**Figure 11.** The depth integrals of net primary production (mg C $m^{-2}$ $day^{-1}$) on 15 September (a) 1980 and (b) 1989.

seasonal difference of 3–4 umol $kg^{-1}$ between nitrate and silicate maxima of AW found by submarine on the upper Chuchi slope during September 1997 (Figures 3c and 3d) and March 1991 [*McRoy*, 1999] and 1995.

[44] Note that in the warmer, less saline ACW of 5°C and 31.5 salinity (Figures 3a and 3b), however, only 0.2 umol $NO_3$ $kg^{-1}$ (Figure 3c), in contrast to 4.1 umol $SiO_4$ $kg^{-1}$ (Figure 3d), were left behind at a phytoplankton biomass of ~1.5 ug chl $l^{-1}$ near 150°W (Figure 3f). A $NO_3$/$SiO_4$ utilization ratio of <0.1, instead of ~1.0 for diatoms [*Brzezinski*, 1985], suggests that nonsiliceous forms were then the dominant functional groups of exiting phytoplankton, within some regions of the Beaufort Sea, during 1997. Here the cyclonic case of the model also yielded a simulated biomass of ~1.5 ug chl $l^{-1}$ at a depth of 60 m near 150°W (Figure 19b), while microflagellates then become the dominant functional group of phytoplankton at ~147°W (Figure 20b), since the competitive advantage of shade-adapted prymnesiophytes was offset by the model's large DOC secretion rate of *Phaeocystis* [*Walsh and Dieterle*, 1994].

[45] *Phaeocystis pouchettii* is now relatively rare (<1 ug chl $l^{-1}$) in shallow regions of the Bering and Chukchi Seas [*Walsh*, 1995], compared with stocks of >10 ug chl $l^{-1}$ within the deeper Greenland and Barents Seas [*Smith et al.*, 1991; *Wassman et al.*, 1990]. Light limitation within deep surface mixed layers (SML) that do no intersect the bottom may favor the shade-adapted prymnesiophytes there [*Sakshaug and Walsh*, 2000] and in Antarctic waters, where spring populations of *Phaeocystis antarctica* bloom first [*Perrin et al.*, 1987; *Davidson and Marchant*, 1992]. They win in deep SML of Southern Ocean models [*Walsh et al.*, 2001; *Arrigo et al.*, 2003], unless significant grazing by protozoans is

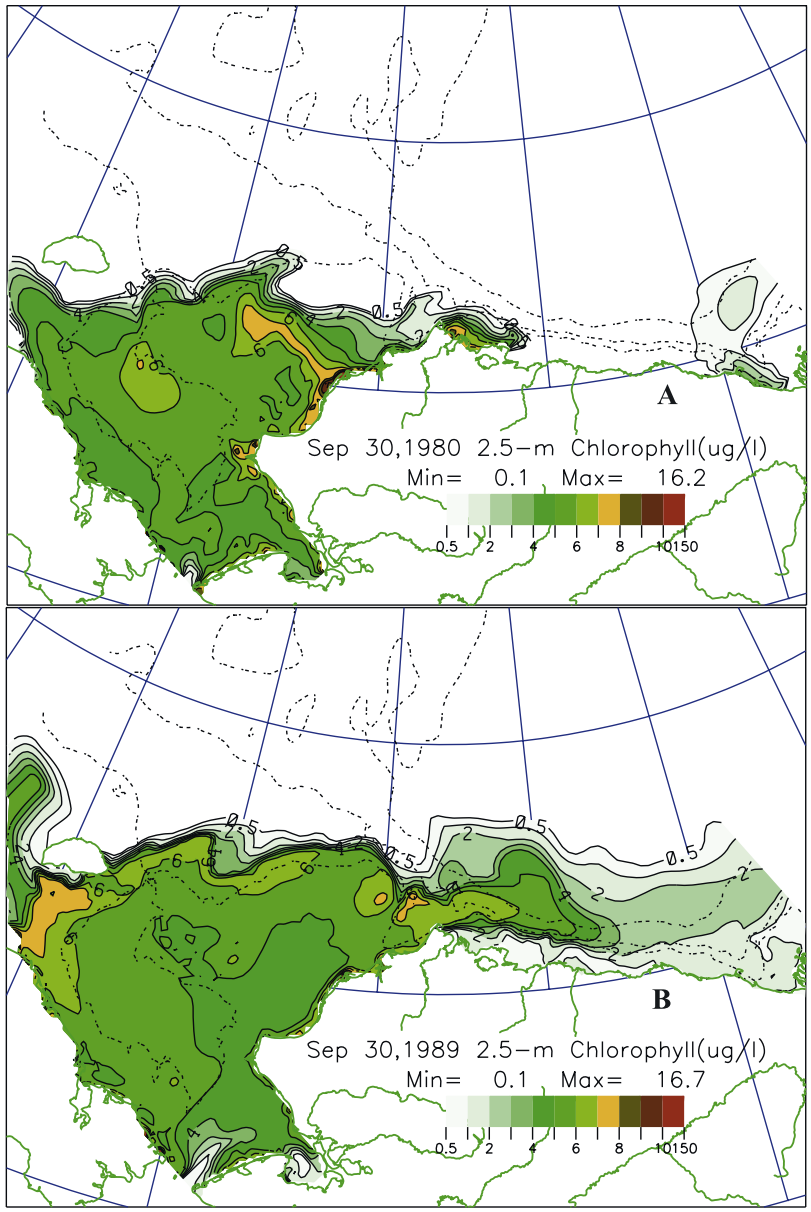


**Figure 12.** The fields of total phytoplankton biomass (ug chl $l^{-1}$) at a depth of 2.5 m on 30 September (a) 1980 and (b) 1989.

imposed on the single-cell stages, after krill disperse the colonial forms [*Walsh et al.*, 2001].

[46] The model's initial condition of protozoan biomass (Table 3) is the maximum value of those usually found in either the Southern Ocean [*Leakey et al.*, 1994] or the southeastern Bering Sea [*Howell-Kubler et al.*, 1996], but the role of local euphausiids in breaking up colonies of *Phaeocystis pouchettii* in the Chukchi/Beaufort Seas is unknown. Since tenfold larger stocks of protozoans were found during the 1999 coccolithophore bloom [*Olson and Strom*, 2002], however, we exerted a maximal grazing loss on the prymnesiophytes, with our assumptions that the single-cell form of *Phaeocystis* ($P_{ps}$) was 90% of their total biomass and thus subject to consumption by protozoan herbivores. Future reductions of ice cover over deeper regions of the Chukchi shelf may thus result in greater utilization of untapped winter nutrients by low light-adapted, poorly-grazed prymnesiophytes [*Matrai et al.*, 1995; *Hansen et al.*, 1994], whose large colonies of 1–2 mm diameter may settle out on the slope, in contrast to the present rain of diatoms at mid-shelf. First, we must account for unknown spring utilization of the winter nutrient fields [*Cooper et al.*, 1997] in a hindcast mode, and then remove all ice cover in a forecast mode, with our next series of coupled model experiments.

## Appendix A: State Equations of the Ecological Models

[47] The ecological models are partitioned in the vertical dimension, z, as a plankton one within an upper water column module of 39 layers of variable thickness, with a maximum bottom depth of 4500-m, and a benthic one, consisting of a well-mixed, 1-cm thick sediment layer. The

18 explicit state variables are defined in Table 1. The processes affecting their change over time, t, and space, x, y, z, are first described by the following equations for the water column, where the parameter values are given in Table 2:

$$\frac{\partial P_d}{\partial t} = Tr(P_d) - \frac{\partial}{\partial z}(w_d P_d) + (g_d - \epsilon_d - \psi_d - \eta_d)P_d - \gamma_d G_c \tag{A1}$$

$$\frac{\partial P_f}{\partial t} = Tr(P_f) - \frac{\partial}{\partial z}(w_f P_f) + \left(g_f - \epsilon_f - \psi_f - \eta_f\right)P_f - \gamma_f G_\mu \tag{A2}$$

$$\frac{\partial P_p}{\partial t} = Tr(P_p) - \frac{\partial}{\partial z}(w_p P_p) + \left(g_p - \epsilon_p - \psi_p - \eta_p\right)P_p - \gamma_p G_\mu \tag{A3}$$

$$\frac{\partial B}{\partial t} = Tr(B) + \frac{(C/N)_b}{(C/N)_r}(g_3 + g_4)B - (\beta + m)B \tag{A4}$$

$$\frac{\partial DOC_1}{\partial t} = Tr(DOC_1) + \sum_i \psi_i P_i - g_3 B + X_2 \tag{A5}$$

$$\frac{\partial DOC_2}{\partial t} = Tr(DOC_2) + \sum_i \eta_i P_i + \eta_c Z_c + \eta_\mu Z_\mu + \phi_c \gamma_d G_c + \phi_\mu(\gamma_f + \gamma_p)G_\mu + \phi_b m B - g_4 B - X_2 \tag{A6}$$

$$\frac{\partial Z_c}{\partial t} = Tr(Z_c) - \frac{\partial}{\partial z}(w_{zc} Z_c) + (1 - \alpha_c - \phi_c)\gamma_d G_c - \eta_c Z_c \tag{A7}$$

$$\frac{\partial Z_\mu}{\partial t} = Tr(Z_\mu) - \frac{\partial}{\partial z}(w_{z\mu} Z_\mu) + (1 - \alpha_\mu - \phi_\mu)(\gamma_p + \gamma_f)G_\mu + (1 - \alpha_b - \phi_b)mB - \eta_\mu Z_\mu \tag{A8}$$

$$\frac{\partial NH_4}{\partial t} = Tr(NH_4) + (N/C)_r\left[\alpha_c \gamma_d G_c + \alpha_\mu(\gamma_p + \gamma_f)G_\mu - \sum_i g_{iNH_4} P_i\right] + (N/C)[\beta + \alpha_b m]B + b\left[(N/C)_b - (N/C)_r\right]\left[(1 - \alpha_b - \phi_b) + \phi_b\right]mB - X_1 \tag{A9}$$

$$\frac{\partial NO_3}{\partial t} = Tr(NO_3) - (N/C)_r \sum_i g_{iNO_3} P_i + X_1 \tag{A10}$$

$$\frac{\partial SiO_4}{\partial t} = Tr(SiO_4) + (Si/C)_r\left[(\alpha_c + \phi_c)\gamma_d G_c + (\eta_d - g_d)P_d + \eta_c Z_c\right] \tag{A11}$$

$$\frac{\partial DIC}{\partial t} = Tr(DIC) + \sum_i (\epsilon_i - g_i)P_i + \alpha_c \gamma_d G_c + \alpha_\mu(\gamma_p + \gamma_f)G_\mu + B(\beta + \alpha_b m) + B(g_3 + g_4)\left(1 - \left[(C/N)_b/(C/N)_r\right]\right) \tag{A12}$$

$$\frac{\partial G_c}{\partial t} = -\frac{\partial u_d G_c}{\partial x} - \frac{\partial v_d G_c}{\partial y} \tag{A13}$$

$$\frac{\partial G_\mu}{\partial t} = -\frac{\partial u_d G_\mu}{\partial x} - \frac{\partial v_d G_\mu}{\partial y}. \tag{A14}$$

[48] The "Tr(..)" terms represent physical advective and diffusive transport:

$$Tr(A) = -\left[\frac{\partial}{\partial x}(uA) + \frac{\partial}{\partial y}(vA) + \frac{\partial}{\partial z}(wA)\right] + \frac{\partial}{\partial z}\left(K_h \frac{\partial A}{\partial z}\right) \tag{A14a}$$

where the last term is the vertical diffusive transport and A is any of the above state variables, except $G_c$ and $G_\mu$. The importance of these advective terms, in relation to the other ones, is considered in the carbon budgets of Figures 23a and 23b. Along the solid coastal boundaries, the horizontal velocities of u, v and mean layer flows of $u_d$, $v_d$ are zero, resulting in a no-flux condition. The vertical velocity, w, is set to zero at the bottom of the water column. Advection through the air-sea interface is also set to zero and no account is taken of the change in the volume of surface grid cells owing to time-dependent free surface height changes. Because of the strong implicit horizontal diffusion in the numerical algorithm for advective transport, we ignore explicit horizontal turbulent mixing and model only the vertical component.

[49] The settling velocities for diatoms and *Phaeocystis*, $w_d$ and $w_p$, are functions of their respective biomass, whereas $w_f$ for microflagellates and $w_{zc}$, $w_{z\mu}$, for copepod and protozoan fecal pellets are constant (Table 2). The subscript "r" refers to the excess of carbon over nitrogen, or carbon over silicon, in all organic matter, except bacteria, where the subscript "b" is used. Subscript "r" denotes the Redfield ratio. These ratios and all other model parameters are given in Table 2.

[50] These parameter values determine, of course, the outcome of competition in this Arctic adaptation of our previous polar model of similar Antarctic phytoplankton communities, in which a prior sensitivity analysis of over 100 simulation cases of the one-dimensional form was performed. Drawing upon extensive field observations of similar genera in the Southern Ocean, we start with an observed light saturation intensity, $I_s$ (Table 2), of 25 watts PAR $m^{-2}$ ($\sim$110 $\mu$E $m^{-2}$ $s^{-1}$) for near-ice stocks of *Phaeocystis* in the Ross Sea [*Palmisano et al.*, 1986], where they outcompete diatoms in deep SML [*Arrigo et al.*, 2003]; their cultures yield maximum net growth rates of $\sim$0.2 $day^{-1}$ at 0.0°C [*Verity et al.*, 1991], as much as 40% excretion rates [*Reid et al.*, 1990], and similar shade-adapted $I_s$ [*Matrai et al.*, 1995].

[51] Since Sun-adapted diatom communities, with higher $I_s$, are instead typical of shallow polar SML of 20–40 m

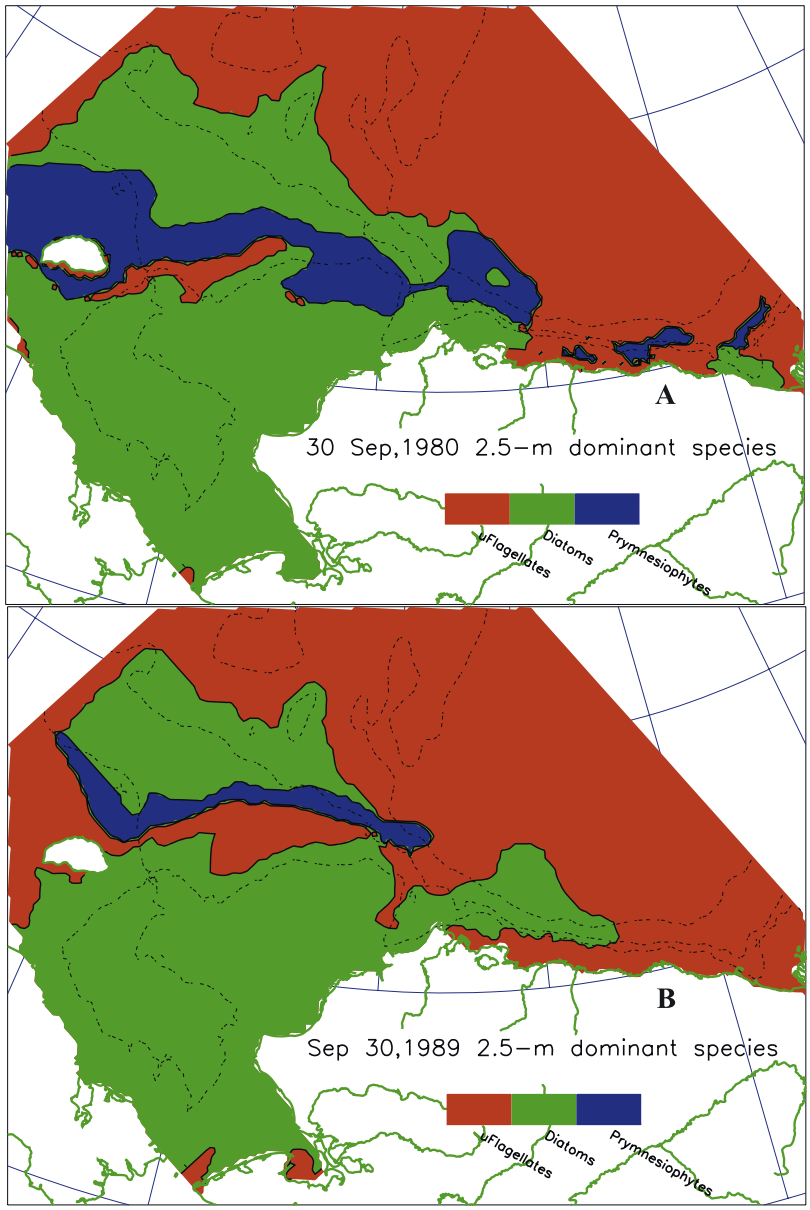


**Figure 13.** The dominance of phytoplankton functional groups of microflagellates, diatoms, and prymnesiophytes at a depth of 2.5 m on 30 September (a) 1980 and (b) 1989.

thickness [*Platt et al.*, 1982; *Sakshaug and Holm-Hansen*, 1986], we instead use 45 watts PAR $m^{-2}$ for this group, as found for the total phytoplankton community of the Barents Sea [*Rey*, 1991] and used in our prior models of the Bering/Chukchi Seas [*Walsh and Dieterle*, 1994; *Walsh et al.*, 1997]. When *Cryptomonas* was the dominant phytoplankton in the Bransfield Strait, however, an intermediate $I_s$ of ~35 watts $m^{-2}$ was observed [*Figueiras et al.*, 1994] compared with higher values of $I_s$ assumed for the model's diatoms and lower ones for *Phaeocystis* (Table 2). We realize that all polar phytoplankton are capable of light-adaptation, with a wide range in realized $I_s$, e.g., much higher values of ~53–66 watts $m^{-2}$ have been found for other culture studies [*Verity et al.*, 1991] and field populations [*Cota et al.*, 1994] of *Phaeocystis*.

[52] Indeed, similar net realized growth rates of both diatoms and *Phaeocystis* in the Barents Sea [*Vernet et al.*, 1998] suggest that their different loss rates will instead determine the outcome of their competition in the "real world" as well as in our model. However, since the ultimate fate of primary production within Arctic food webs, production of muscilaginous DOC by *Phaeocystis* colonies or consumption of diatoms by copepods, may be determined by which functional group dominates the base of the food web [*Sakshaug and Walsh*, 2000], we wished to explore which future western Arctic habitats, if any, might favor the shade-adapted prymnesiophytes of the Southern Ocean [*Walsh et al.*, 2001; *Arrigo et al.*, 2003], the Greenland Sea [*Cota et al.*, 1994], and the Barents Sea [*Sakshaug*, 2004].

[53] Most diatoms have relatively low excretion rates of ~4% [*Reid et al.*, 1990], but their respiration rates may be as much as ~19% of the daily gross production at ~1.5°C in mesocosms [*Keller and Riebesell*, 1989]. Indeed, using

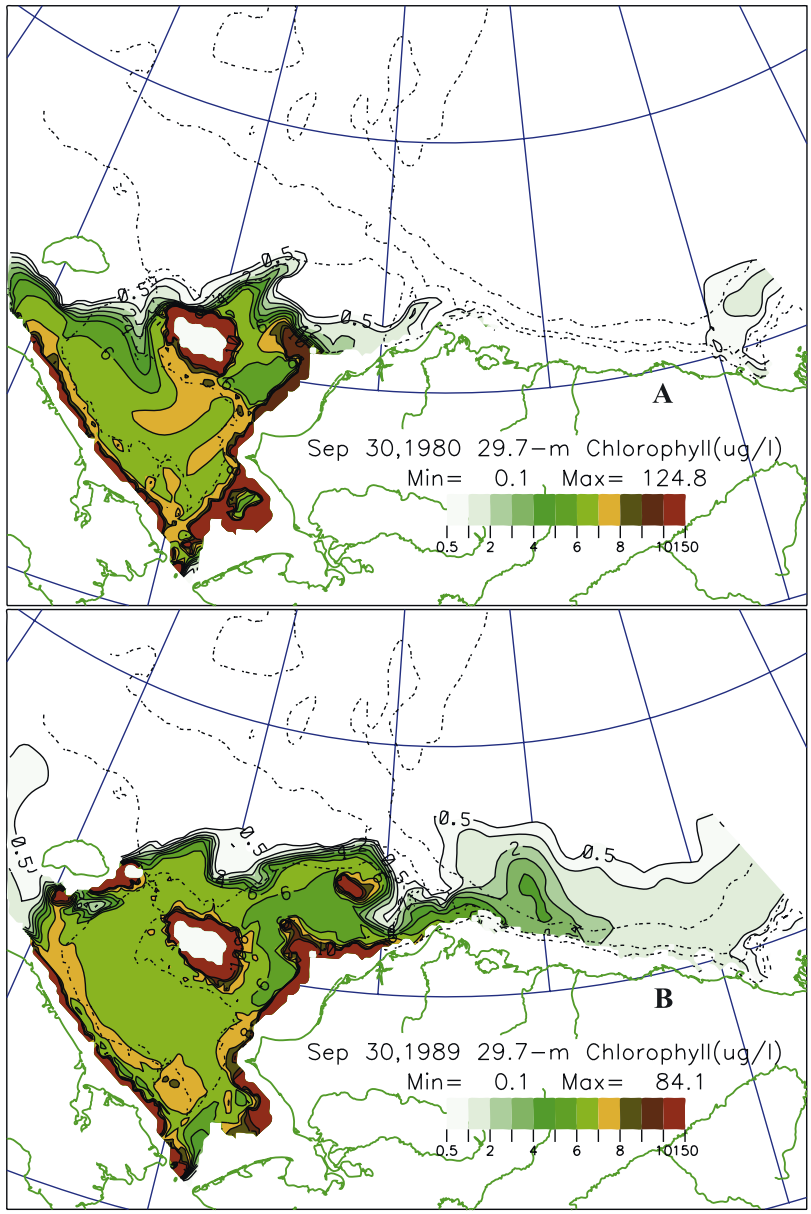


**Figure 14.** The fields of total phytoplankton biomass (ug chl $l^{-1}$) at a depth of ~30 m on 30 September (a) 1980 and (b) 1989.

measured depth-integrals of the respiration rates [*Aristegui and Montero*, 1995] of their field populations in Bransfield Strait, a prior budget [*Walsh et al.*, 2001] of their respiratory demands, in addition to their assumed small DOC fluxes to assess the likely values of $\epsilon_i$ and $\psi_i$ within equations (A1)–(A3), (A5)–(A6), and (A12), found that a respiration flux of as much as ~20% of their gross primary production was required. We assume a conservative respiration rate of 10% for diatoms, and lower values of respiration for the more shade-adapted flagellates and prymnesiophytes in this analysis (Table 2).

[54] Finally, within the sediment layer, the state variables of non-siliceous and siliceous particulate sediment carbon, $S_p$ and $S_{ps}$, are both described by:

$$\frac{\partial S_{p,ps}}{\partial t} = K_b \frac{\partial^2 S_{p,ps}}{\partial z_s^2} - \lambda S_{p,ps} \qquad \text{(A15) – (A16)}$$

where $K_b$ is the bioturbation coefficient and $\lambda$ is the decay constant. $K_b$ is a function of bottom temperature [*Walsh and Dieterle*, 1994], supplied by the physical model.

[55] The last two state variables of sediment dissolved inorganic carbon and silicate are governed by:

$$\frac{\partial Ds}{\partial t} = K_m \frac{\partial^2 Ds}{\partial z_s^2} + \lambda S_p + \lambda S_{ps} \qquad \text{(A17)}$$

$$\frac{\partial DSIO_4}{\partial t} = K_m \frac{\partial^2 DSIO_4}{\partial z_s^2} + \lambda S_{ps}, \qquad \text{(A18)}$$

where $K_m$ is the porewater molecular diffusivity (Table 2). As described in the section on vertical boundary conditions, dissolved recycled nitrogen, i.e., ammonium and nitrate, in the sediments are implicit variables, assuming a Redfield C/N ratio of source Ds + DOC/DON.

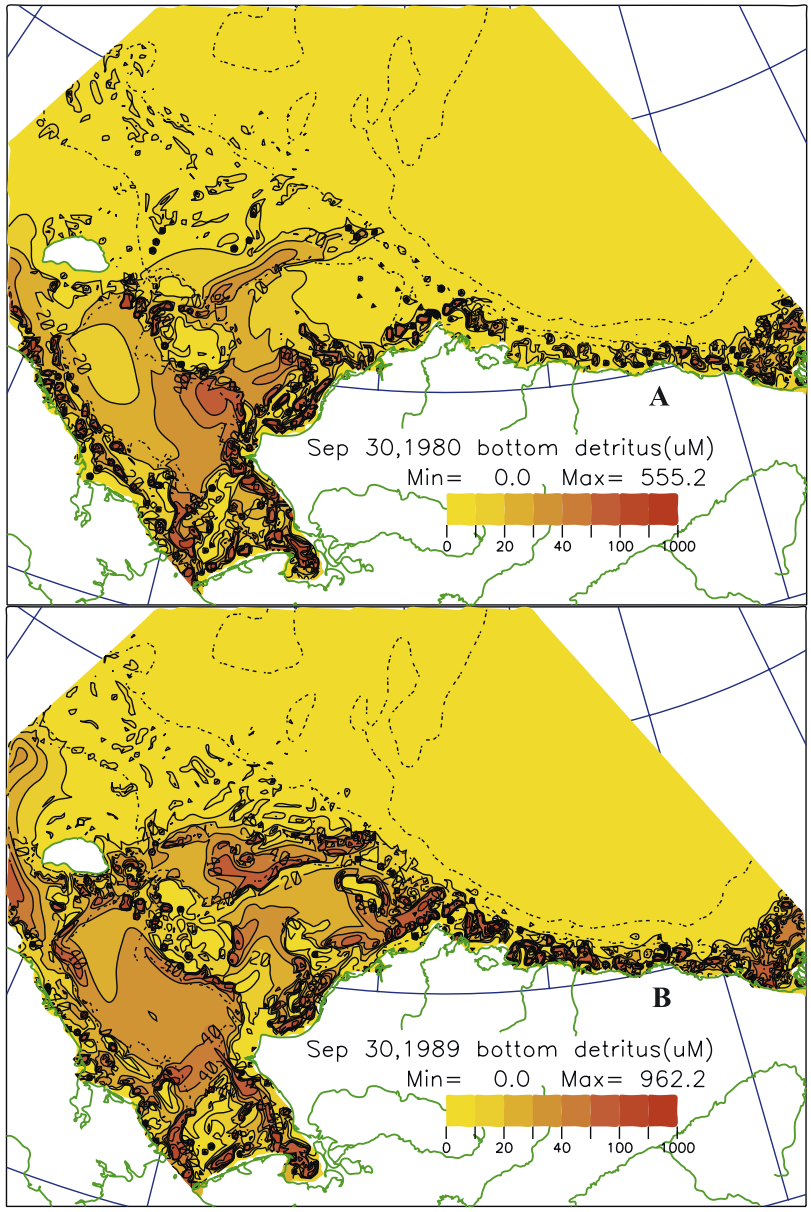


**Figure 15.** The fields of bottom debris (umol C $kg^{-1}$) of phytodetritus and fecal pellets of copepod, protozoan, and carnivorous origin on 30 September (a) 1980 and (b) 1989.

[56] The algal growth terms of equations (A1)–(A3) and (A9)–(A12) are given by

$$g_i = \min\left[c_i \frac{L(t,z)}{L_{is}} \exp\left(1 - \frac{L(t,z)}{L_{is}}\right), g_{i,N}, g_{i,sio_3}\right] \quad \text{(A19)}$$

$$g_{i,N} = c_i \max\left[\frac{NO_3}{k_{iNO_3} + NO_3}, \frac{NH_4}{k_{iNH_4} + NH_4}\right] \quad \text{(A20)}$$

$$g_{i,SIO_4} = c_i \frac{SIO_4}{k_{iSIO_4} + SIO_4}, \quad \text{(A21)}$$

where subscript "i" is d, f, or p for diatoms, microflagellates, and *Phaeocystis* respectively. The maximum growth rates of each functional group, $c_i$, are functions of temperature [*Epply*, 1972]. The half saturation constants, $k_{iNO_3}$, $k_{iNH_4}$, and $k_{iSIO_4}$, for the three groups are given in Table 2, as is the Si/C ratio of diatoms [*Brzezinski*, 1985].

[57] Ice may overly only a fraction of the 9-km wide model grid cells. Thus the light-regulated component of phytoplankton growth within any model grid cell is calculated as the weighted averaged of their growth in open water, multiplied by the percentage of open water in the grid cell, and their growth under ice, multiplied by the percentage of ice cover.

[58] In open water, the fraction of surface PAR penetrating to depth, z, is described [*Fasham et al.*, 1983; *Taylor et al.*, 1991] by:

$$I_w(z) = \left[R_b e^{-(k_b(w)+k_m)z} + (1 - R_b)e^{-k_r(w)z}\right] e^{-k_c z} \quad \text{(A22)}$$

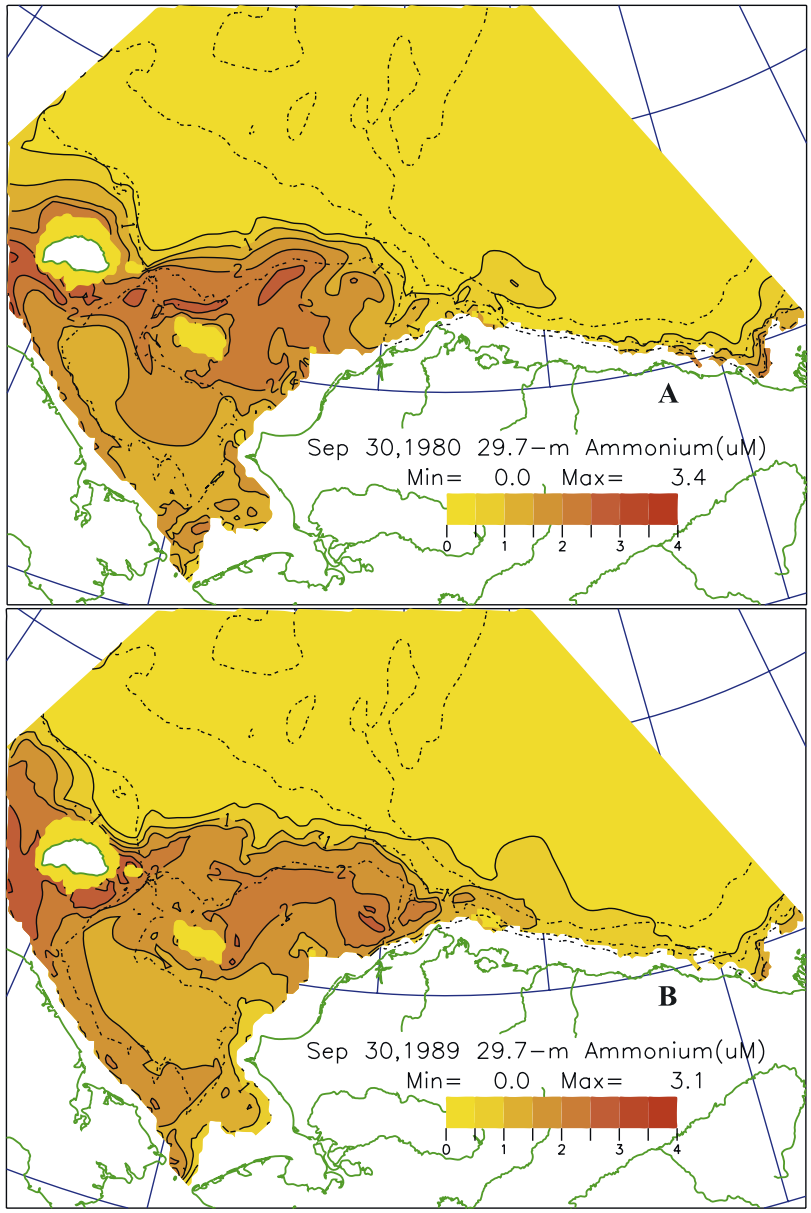


**Figure 16.** The fields of ammonium (umol $NH_4$ $kg^{-1}$) at a depth of ~30 m on 30 September (a) 1980 and (b) 1989.

where $R_b$ is the fraction of surface light in the blue-green wavelengths. The attenuation coefficients $k_m$ and $k_c$ are computed as

$$k_m = \frac{k_y}{z}\int_0^z (DOC_1 + DOC_2)dz \tag{A23}$$

$$k_c = \frac{1}{z}\int_0^z \left(k_d P_d + k_f P_f + k_p P_p\right)dz, \tag{A24}$$

with the values of the other attenuation coefficients, and $R_b$, given in Table 2.

[59] Ice is assumed to be capped by a layer of snow, with a layer of ice algae at its undersurface [*Smith*, 1995]. The fraction of light penetrating to the water interface is given by:

$$I_{ice} = \left[R_b e^{-[k_b(s)z(s)+k_b(i)z(i)]} + (1-R_b)e^{-[k_r(s)z(s)+k_r(i)z(i)]}\right]e^{-k(a)z(a)}, \tag{A25}$$

where the attenuation coefficient for ice algae, k (a), is set to 0.38 $m^{-1}$ and z (a) = 1 cm [*Smith*, 1995]. The attenuation coefficients for blue-green and red light in ice and snow are 2,15 $m^{-1}$ and 4, 35 $m^{-1}$ respectively [*Wadhams*, 2000]. Snow and ice thicknesses are set at 2.0 and 0.1 m respectively. Given this set of snow/ice parameters, only 0.2% of surface PAR passes through to the surface of the model's water column when covered by ice (Figure 10).

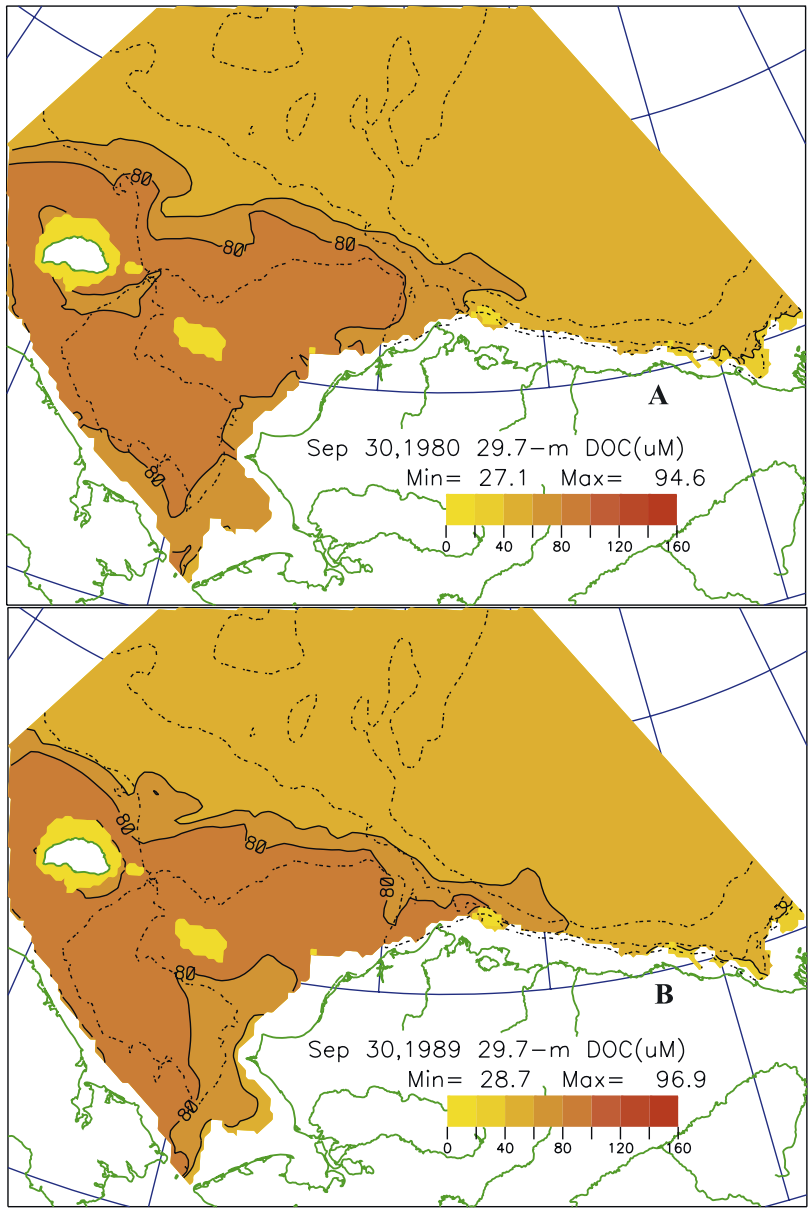


**Figure 17.** The fields of the sum of monomeric and macromolecular dissolved organic carbon (umol DOC $kg^{-1}$) at a depth of ~30 m on 30 September (a) 1980 and (b) 1989.

[60] The daily average PAR, $I_p$, was first prescribed as a function of latitude and longitude, using 50% of the NCEP reanalysis [*Kistler et al.*, 2001] monthly mean net surface shortwave fluxes. These were interpolated to the model grid from the coarser 2.5 degree resolution of the NCEP data set. The ice fields were also interpolated from the end-of-month sea-ice cover distributions [*Chapman and Walsh*, 1993], with an Arctic resolution of 60 nautical miles.

[61] Light at the surface is also a function of time of day. It was next calculated, assuming a sinusoidal distribution over the photoperiod as

$$L(t,0) = I_m \sin(\pi t_s/\Delta) \tag{A26}$$

where $t_s$ is time since sunrise, $\Delta$ is the photoperiod, $0 < t_s/\Delta < 1$, and $I_m = 24\ I_p(\pi/2\Delta)$. The light field at depth, z, in each algal growth term is $L(t, z) = L(t, 0)I_w$ for open water, and $L(t, z) = L(t, 0)I_wI_{ice}$ under ice.

[62] The bacterial growth terms, $g_3$, $g_4$, of equations (A4), (A7), and (A8) are

$$g_3 = c_b \frac{DOC_1}{k_{DOC} + DOC_1} \tag{A27}$$

$$g_4 = 0.4c_b \frac{DOC_2}{k_{DOC} + DOC_2}, \tag{A28}$$

where the half-saturation constant $k_{DOC}$ is 0.83 umol $kg^{-1}$ (Table 2). The maximum bacterial growth rate, $c_b$, is a function of temperature as is bacterial mortality, m (Table 2). Only 40% of the macromolecular $DOC_2$ is

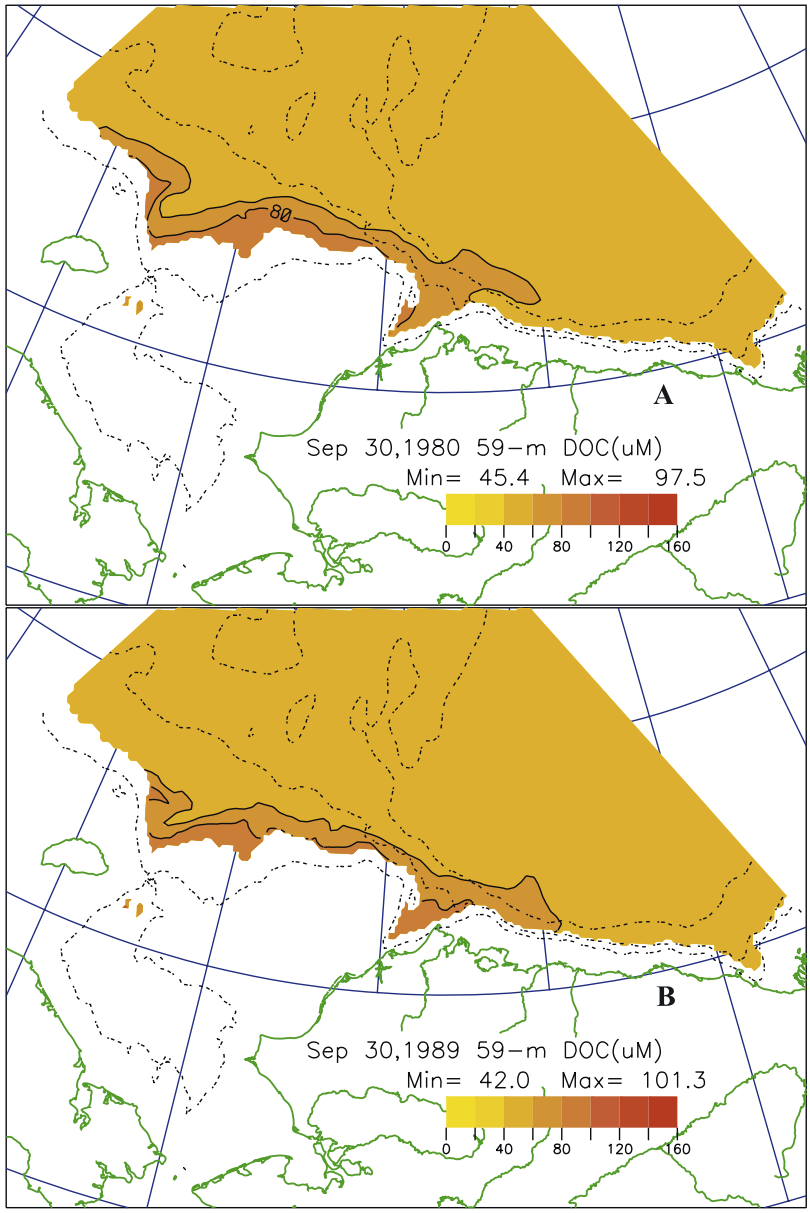


**Figure 18.** The fields of the sum of monomeric and macromolecular dissolved organic carbon (umol DOC $kg^{-1}$) at a depth of ~60 m on 30 September (a) 1980 and (b) 1989.

considered to be labile [*Walsh and Dieterle*, 1994]. The photolysis of $DOC_2$ to more usable $DOC_1$, $X_2$, is a zero order rate term applied in the upper 5 m of the water column within open water during daylight hours (Table 2).

[63] Grazer stocks, $G_c$ and $G_\mu$, change only through advection by the mean layer flow, $u_d$, $v_d$, since their biological growth and loss processes are assumed to be in balance and they may migrate daily over the water column. The rate at which diatoms are grazed, $\gamma_d$, (Table 2), is twice the daily ration (as percent body carbon) of copepods, $G_c$, because 50% of the food encountered is presumed to be lost during "sloppy feeding." Copepod grazing is restricted to the upper 200-m of the model's water column.

[64] Protozoans, $G_\mu$, graze both microflagellates and single-cell *Phaeocystis* ($P_{ps}$). In these scenarios, $P_{ps}$ is assumed to be 90% of the total *Phaeocystis* biomass to impose maximal grazing losses on the prymnesiophytes [*Walsh et al.*, 2001]. The daily ration of protozoans changes as a function of food availability, $\gamma_\mu = \zeta(P_f + P_{ps})$, where $\zeta$ is in units of umole $kg^{-1}$ $day^{-1}$. They graze the most abundant food first, and then the least abundant prey item to satisfy their food requirements. Protozoan grazing is restricted to the upper 100 m of the water column. No grazing by protozoans or by copepods is imposed on algal concentrations of less than 0.05 ug chl $l^{-1}$ of each algal group to establish prey refugia.

[65] The nitrification rate, $X_1$, in the water column is expressed by

$$X_1 = 0.04\left(\frac{NH_4}{k_{NIT} + NH_4}\right) \tag{A29}$$

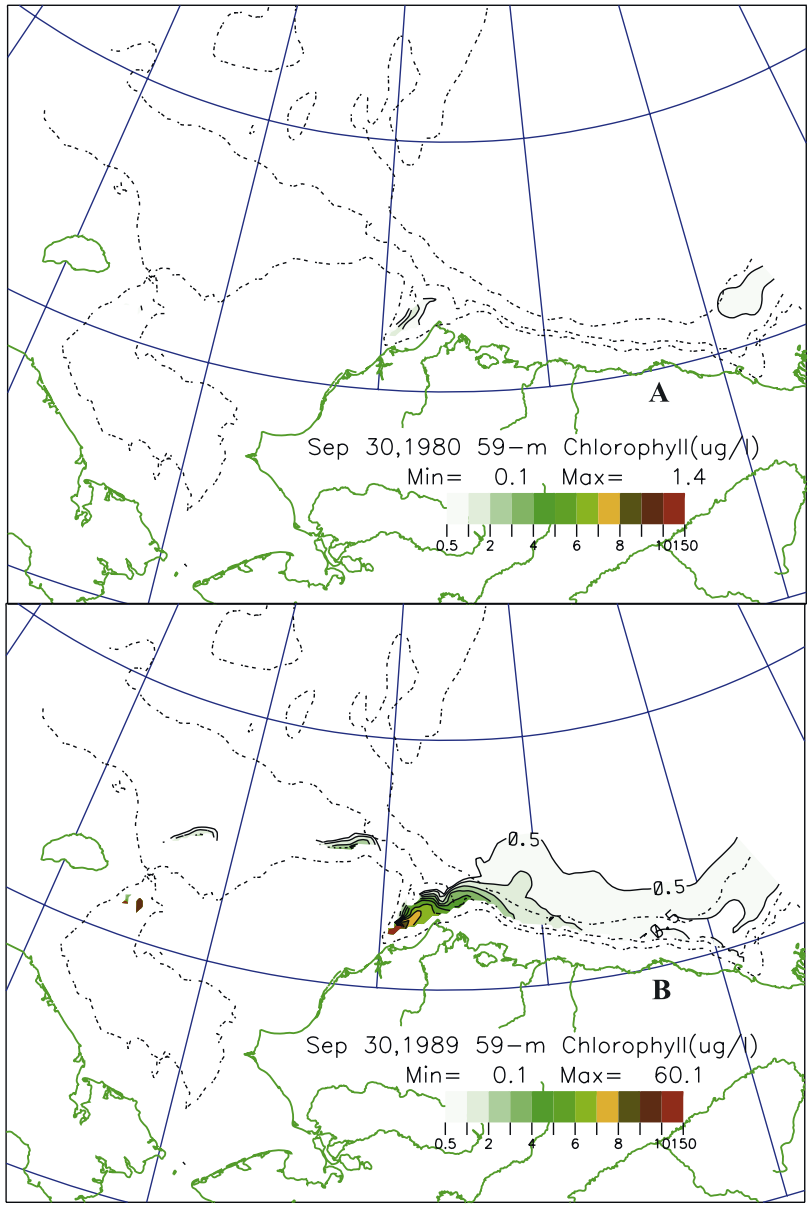


**Figure 19.** The fields of total phytoplankton biomass (ug chl $l^{-1}$) at a depth of ~60 m on 30 September (a) 1980 and (b) 1989.

where 0.04 umole N kg $^{-1}$ day$^{-1}$ is the maximum rate [*Walsh and Dieterle*, 1994]. In the sediments, benthic nitrification is assumed to be 20% of the DON released from PON sources of the settling phytodetritus and fecal pellets that survive descent though the water column.

## A1. Boundary Conditions in z

[66] The settling velocities of equations (A1)–(A3) and (A7)–(A8) are identically zero at the air-sea and water-sediment interfaces. The diffusive fluxes are also set to zero at the air-sea interface in equations (A1)–(A11), whereas for equation (A12),

$$\left(K_h \frac{\partial DIC}{\partial z}\right)_0 = W_{gas} C_{co_2} \left[(pCO_2)_{air} - (pCO_2)_0\right], \qquad \text{(A30)}$$

where $W_{gas}$ = 5.55 × $10^{-5}$ m $s^{-1}$ is the piston velocity for open water, assuming a wind speed of 5 m $s^{-1}$. The piston velocity for gas transfer through ice is assumed to be 25% of the open water value, such that the total flux is a weighted average over open water and under ice cover.

[67] The model's partial pressure of $CO_2$ in air $(pCO_2)_{air}$ is constant at 365 uatm, similar to that observed in September 2000 [*Murata and Takizawa*, 2003]. In the top layer of the water column $(pCO_2)_0$, as well as the solubility of $CO_2$ in seawater, $C_{co2}$, is calculated [*Peng et al.*, 1987] as a function of temperature and salinity. For the alkalinity we assume a constant value of 2200 ueq $kg^{-1}$ over the model domain, which corresponds to a salinity of 31.82, if alkalinity is related to salinity, S, by 2419.7 (S/35)[*Murata and Takizawa*, 2003].

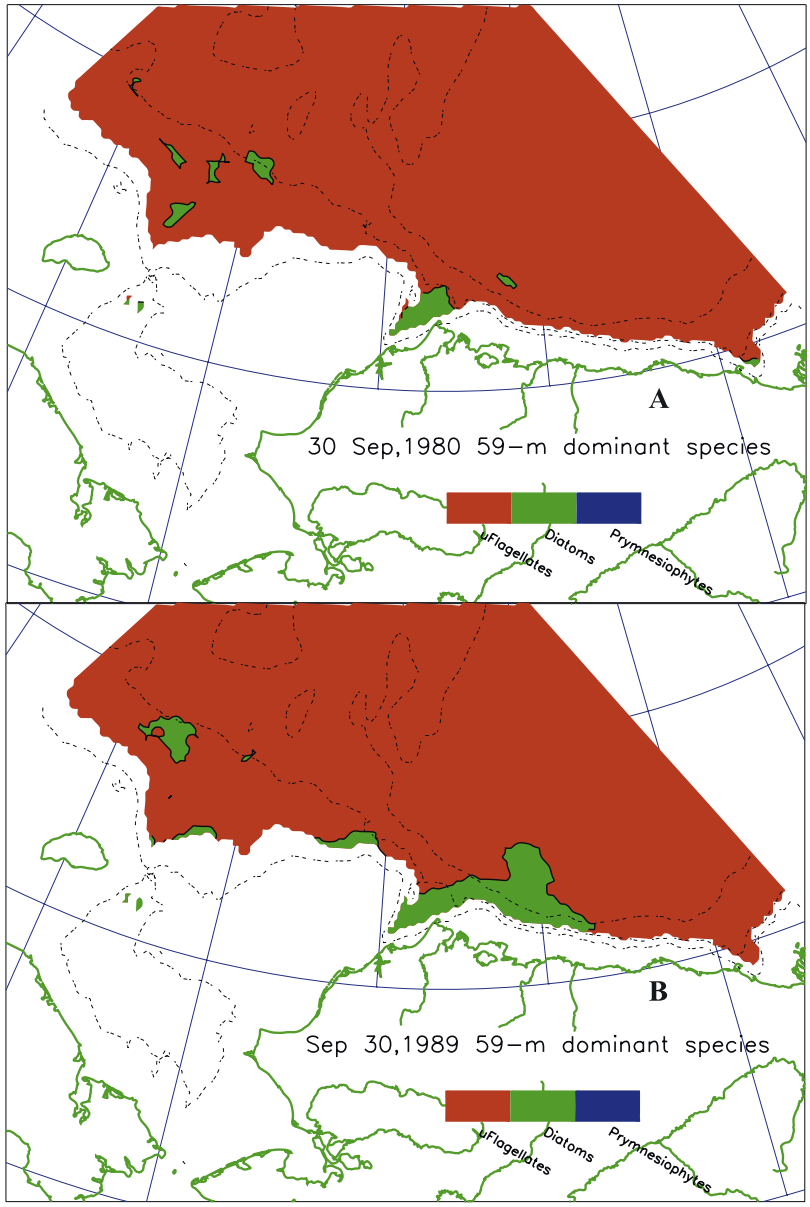


**Figure 20.** The dominance of phytoplankton functional groups of microflagellates, diatoms, and prymnesiophytes at a depth of ~60 m on 30 September (a) 1980 and (b) 1989.

[68] A global relationship of salinity and alkalinity [*Millero et al.*, 1998] was initially employed, because it matched the Arctic Ocean Section (Figure 1) data quite well [*Swift et al.*, 1997]. Surface salinity of the physical model ranged over ~18.5 to ~32.5, however, such that the calculated pCO2 values were out of range. We obtained more reasonable results, by assuming a constant salinity of ~32 for our pCO2 calculations. A salinity of 32 yields an alkalinity of about 2200 from prior observations [*Murata and Takizawa*, 2003; *Fransson et al.*, 2001].

[69] At the water-sediment interface, the boundary conditions for equations (A2)–(A3) and (A8) are

$$K_h \frac{\partial A}{\partial z} = K_b \frac{\partial S_p}{\partial z_s} = K_b \frac{[S_p(w) - S_p]}{0.5[dz(w) + dz(s)]} \frac{A(d)}{S_p(w)} \quad \text{(A31)} - \text{(A33)}$$

where A is either $P_f$, $P_p$, or $Z_\mu$. Here, A(d) is the value in the bottom layer of the water column, while $S_p(w) = (P_f(d) + P_p(d) + Z_\mu(d))$, dz(w) is the thickness of the bottom layer in the water column, and dz(s) is the thickness of the sediment layer.

[70] Similarly, for equations (A2) and (A7):

$$K_h \frac{\partial A}{\partial z} = K_b \frac{\partial S_{ps}}{\partial z_s} = K_b \frac{[S_{ps}(w) - S_{ps}]}{0.5[dz(w) + dz(s)]} \frac{A(d)}{S_{ps}(w)}, \quad \text{(A34)} - \text{(A35)}$$

where A is $P_d$ or $Z_c$. Particulate material is constrained to move from the water column to the sediments via mixing from bioturbation, $K_b$ as a function of the model's bottom temperature (Table 2), such that at shelf temperatures of −1.8°C to + 6.3°C (Figure 7), the biotic inward transport of debris on the Chukchi shelf is always at a bioturbation rate of >0.1 $cm^2$ $yr^{-1}$ [*Smith et al.*, 2003], while particulate fluxes directed out of the sediment are set to zero, i.e., ignoring resuspension events.

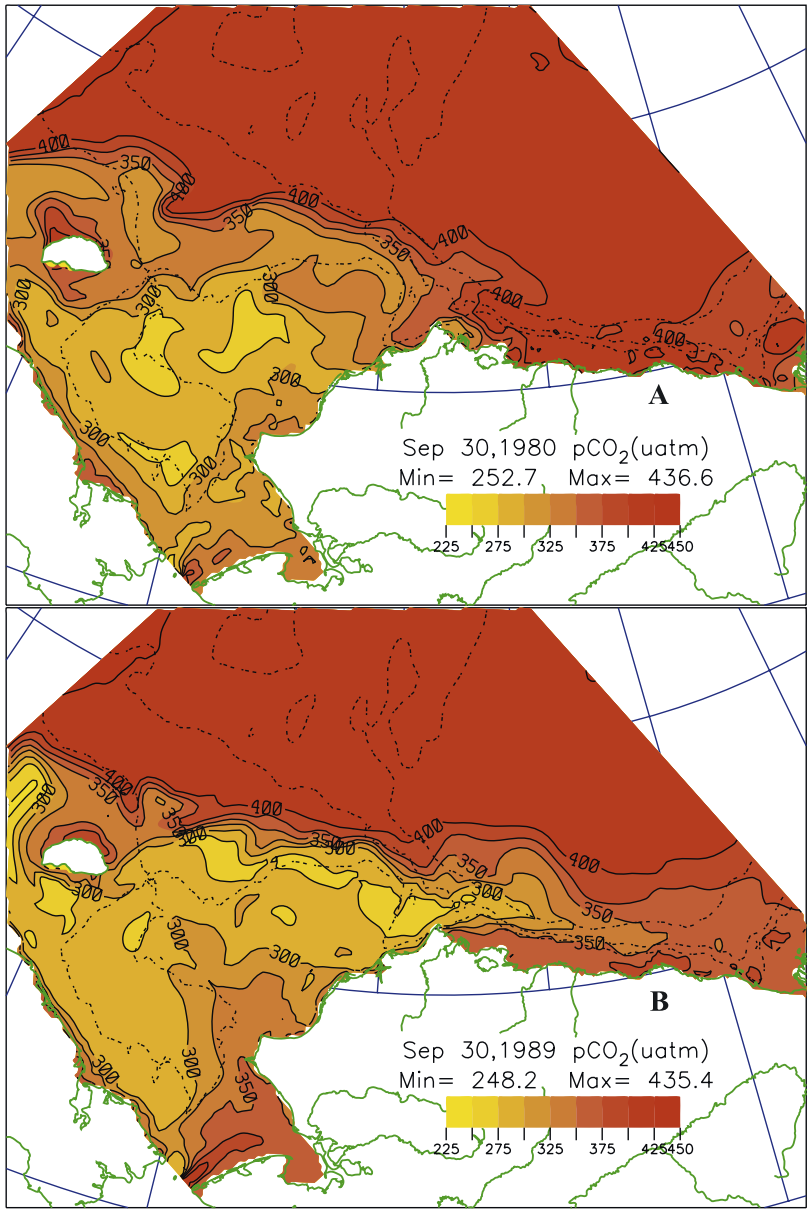


**Figure 21.** The partial pressure (utam) of carbon dioxide ($pCO_2$) within surface sea water on 30 September (a) 1980 and (b) 1989.

[71] Sediment dissolved organic carbon is assumed to be macromolecular $DOC_2$, such that the flux of monomeric $DOC_1$ from the sediments is zero. The $DOC_2$ flux for the lower boundary condition of equation (A6) is

$$K_h \frac{\partial DOC_2}{\partial z} = K_m \frac{\partial Ds}{\partial z_s} = K_m \frac{[DOC_2(w) - Ds]}{0.5[dz(w) + dz(s)]} \qquad \text{(A36)}$$

where $DOC_2$(w) is again the concentration of $DOC_2$ in the bottom layer of the water column.

[72] The bottom condition on silicate of equation (A11) is similarly

$$K_h \frac{\partial SIO_4}{\partial z} = K_m \frac{\partial DSIO_4}{\partial z_s} = K_m \frac{[SIO4(w) - DSIO_4]}{0.5[dz(w) + dz(s)]}. \qquad \text{(A37)}$$

The flux of DIC from the sediments is set equal to the flux of $DOC_2$ to satisfy the boundary condition of equation (12). Assuming a Redfield balance of nitrogen to carbon atoms, the lower boundary conditions of equation (9) and (10) are also described by:

$$K_h \frac{\partial NH_4}{\partial z} = f_s(NH_4)\left[(N/C)_r K_h \frac{\partial DIC}{\partial z}\right] \qquad \text{(A38)}$$

$$K_h \frac{\partial NO_3}{\partial z} = f_s(NO_3)\left[(N/C)_r K_h \frac{\partial DIC}{\partial z}\right], \qquad \text{(A39)}$$

where $f_s(NH_4) = 0.8$ and $f_s(NO_3) = 0.2$, i.e., ammonification is the main fate of DON in the model sediments. The fluxes out through the bottom of the sediment layer are zero for all

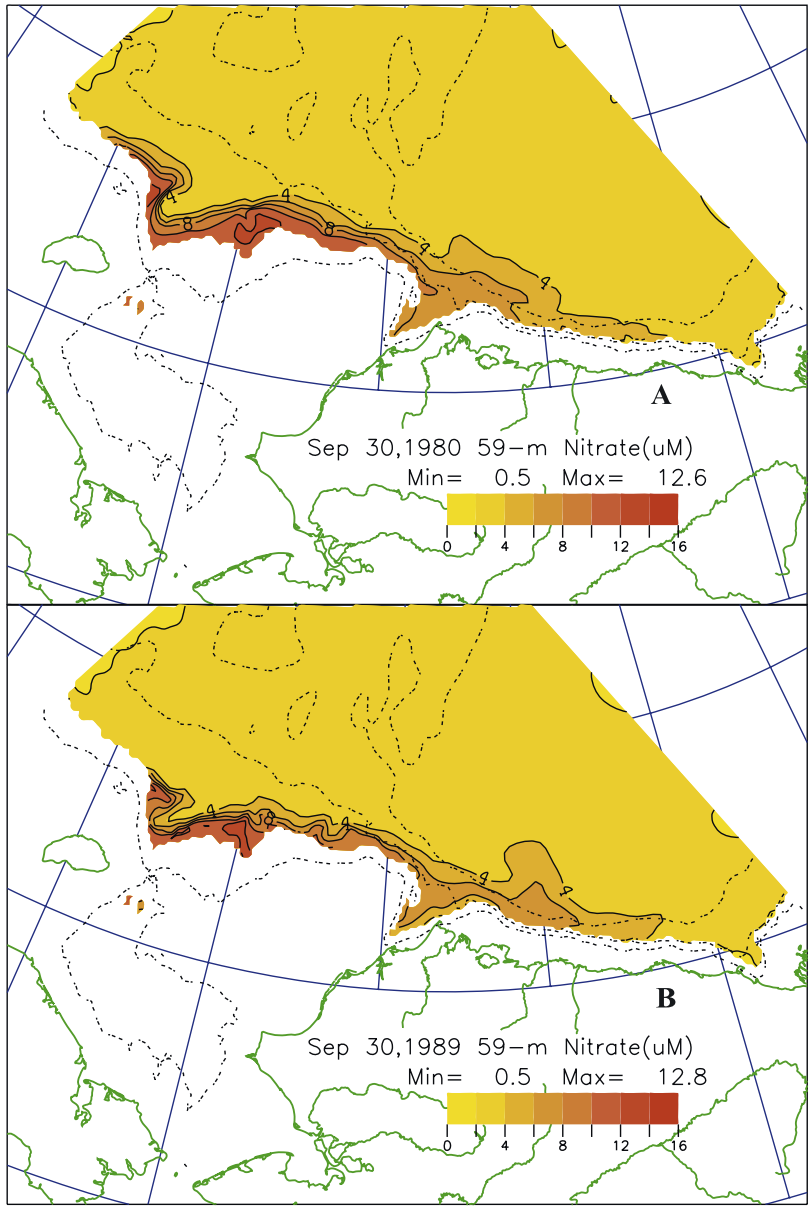


**Figure 22.** The fields of nitrate (umol $NO_3$ $kg^{-1}$) at a depth of ~60 m on 30 September (a) 1980 and (b) 1989.

variables, i.e., ignoring long-term burial [*Banahan and Goering*, 1986; *Smith et al.*, 2003].

## A2. Initial Conditions: Sediment Layer

[73] The horizontal boundary conditions, as well as the initial conditions of variables in the water column, are given in Table 3. Within the sediments, the initial conditions for particulate carbon are $S_p = S_p(w)$ and $S_{ps} = S_{ps}(w)$. Initial values for interstitial DIC, Ds, and silicate, $DSIO_4$, beneath the Anadyr Plume are calculated from

$$Ds = DOC_2(w) - 6.0/\{K_m/(0.5[dz(w) + dz(s)])\} \quad (A40)$$

$$DSIO_4 = SIO_4(w) - 0.7/\{K_m/(0.5[dz(w) + dz(s)])\} \quad (A41)$$

Elsewhere, they are

$$Ds = DOC_2(w) - 1.0/\{K_m/(0.5[dz(w) + dz(s)])\} \quad (A42)$$

$$DSIO_4 = SIO_4(w) - 0.15/\{K_m/(0.5[dz(w) + dz(s)])\} \quad (A43)$$

[74] The initial sediment effluxes of 6.0 mmole C $m^{-2}$ $day^{-1}$ or a nitrogen flux of 0.9 mmole N $m^{-2}$ $day^{-1}$ (0.7 mmole $NH_4$ $m^{-2}$ $day^{-1}$ + 0.2 mmole $NO_3$ $m^{-2}$ $day^{-1}$) assume a Redfield ratio, using previous measurements [*Walsh et al.*, 1989; *Henriksen et al.*, 1993; *Devol et al.*, 1997], as well as observations of 0.7 mmole $SiO_4$ $m^{-2}$ $day^{-1}$ [*Banahan and Goering*, 1986]. Lower initial nutrient fluxes were assumed for the remainder of the model's domain, underlying nutrient-poor Alaska Coastal Water.

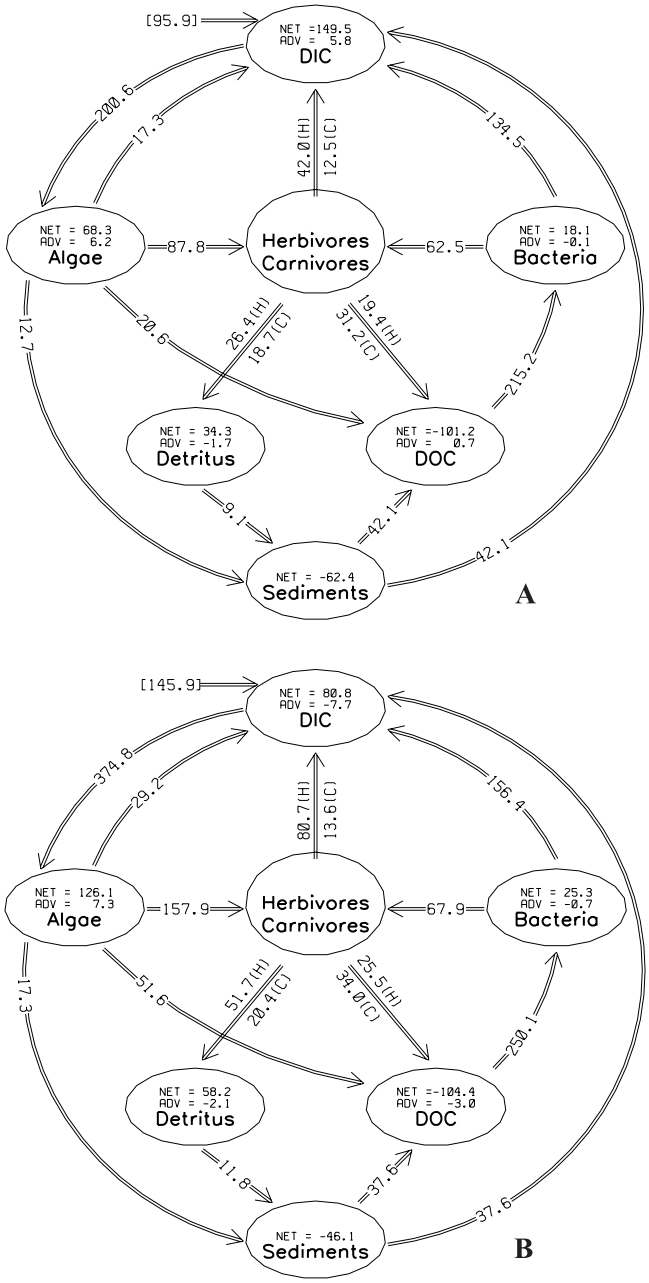


**Figure 23.** Daily carbon budgets (mg C $m^{-2}$ $day^{-1}$) for the Chukchi/Beaufort shelves of <220 m depth, averaged over the month of September (a) 1980 and (b) 1989. The numbers in brackets are the air-sea fluxes, while the herbivore-regulated and carnivore-regulated fluxes between the model pools of the sum of functional groups of microalgae, bacteria, water column detritus, DOC, DIC, and sediment debris are denoted by H and C, respectively.

[75] **Acknowledgments.** This analysis was funded by grants OPP-0124864 to JJW and OPP-0124943 to WM from the National Science Foundation as part of the joint SBI project "Collaborative Research: Carbon Cycling in the Chukchi and Beaufort Seas-Field and Modeling Studies."

## References

Aagaard, K., R. Woodgate, and T. Weingartner (2002), Bering Strait: Gateway to the Arctic, Polar Sci. Cent., Seattle, Wash. (Available at http://psc.apl.washington.edu)

Amon, R. M., and R. Benner (2003), Combined neutral sugars as indicators of the diagenetic state of dissolved organic matter in the Arctic Ocean, *Deep Sea Res.*, *50*, 151–170.

Aristegui, J., and M. F. Montero (1995), Plankton community respiration in Bransfield Strait (Antarctic Ocean) during austral spring, *J. Plankt. Res.*, *17*, 1647–1660.

Arrigo, K. R., D. L. Worthen, and D. H. Robinson (2003), A coupled ocean-ecosystem model of the Ross Sea: 2. Iron regulation of phytoplankton taxonomic variability and primary production, *J. Geophys. Res.*, *108*(C7), 3231, doi:10.1029/2001JC000856.

Banahan, S., and J. J. Goering (1986), Biogenic silica on the SE Bering shelf, *Cont. Shelf Res.*, *5*, 199–214.

Barnard, W. R., M. O. Andreae, and R. L. Iversen (1984), Dimethylsulfide and Phaeocystis pouchetii in the southeastern Bering Sea, *Cont. Shelf Res.*, *3*, 103–113.

Belicka, L. L., R. W. Macdonald, and H. R. Harvey (2002), Sources and transport of organic carbon to shelf, slope, and basin surface sediments of the Arctic Ocean, *Deep Sea Res.*, *49*, 1463–1484.

Berge, G. (1962), Discoloration of the sea due to Coccolithus huxleyi "bloom," *Sarsia*, *6*, 27–40.

Booth, B. C., and R. A. Horner (1997), Microalgae on the Arctic Ocean section, 1994: Specie abundance and biomass, *Deep Sea Res.*, *44*, 1607–1622.

Brzezinski, M. A. (1985), The Si:C:N ratio of marine diatoms: Interspecific variability and the effect of some environmental variables, *J. Phycol.*, *2*, 347–357.

Carmack, E. C., K. Aagaard, J. H. Swift, R. W. Macdonald, F. A. McLaughlin, E. P. Jones, R. G. Perkin, J. N. Smithj, K. M. Ellis, and L. R. Kilius (1997), Changes in temperature and tracer distributions with the Arctic Ocean: Results from the 1994 Arctic Ocean Section, *Deep Sea Res.*, *44*, 1487–1502.

Chapman, W. L., and J. E. Walsh (1993), Recent variations of sea ice and air temperature in high latitudes, *Bull. Am. Meteorol. Soc.*, *74*, 33–48.

Coachman, L. K. (1993), On the flow field in the Chirikov Basin, *Cont. Shelf Res.*, *13*, 481–508.

Coachman, L. K., and K. Aagaard (1988), Transport through Bering Strait: Annual and interannual variability, *J. Geophys. Res.*, *93*, 15,535–15,539.

Codispoti, L. A., and F. A. Richards (1968), Micronutrient distributions in the East Siberian and Laptev Seas during summer 1963, *Arctic*, *21*, 67–83.

Codispoti, L. A., G. E. Friederich, and D. W. Hood (1986), Variability of the inorganic carbon system over the SE Bering Sea shelf during spring 1980 and spring-summer 1981, *Cont. Shelf Res.*, *5*, 133–160.

Cooper, L. W., T. E. Whitledge, J. M. Grebmeier, and T. Weingartner (1997), The nutrient, salinity, and stable oxygen isotope composition of Bering and Chukchi Seas waters in and near the Bering Strait, *J. Geophys. Res.*, *102*, 12,563–12,573.

Cota, G. F., W. O. Smith, and B. G. Mitchell (1994), Photosynthesis of *Phaeocystis* in the Greenland Sea, *Limnol. Oceanogr.*, *39*, 948–953.

Cota, G. F., L. R. Pomeroy, W. G. Harrison, E. P. Jones, F. Peters, W. M. Sheldon Jr., and T. R. Weingartner (1996), Nutrients, primary production and microbial heterotrophy in the southeastern Chukchi Sea: Arctic summer nutrient depletion and heterotrophy, *Mar. Ecol. Prog. Ser.*, *135*, 247–258.

Davidson, A. T., and H. J. Marchant (1992), Protist abundance and carbon concentration during a *Phaeocystis*-dominated bloom at an Antarctic coastal site, *Polar Biol.*, *12*, 387–395.

Devol, A. H., L. A. Cidispoti, and J. P. Christensen (1997), Summer and winter denitrification rates in western Arctic shelf sediments, *Cont. Shelf Res.*, *9*, 1029–1050.

Epply, R. W. (1972), Temperature and phytoplankton growth in the sea, *Fish. Bull.*, *70*, 1063–1085.

Fasham, M. J., P. M. Holligan, and P. R. Pugh (1983), The spatial and temporal development of the spring phytoplankton bloom in the Celtic Sea, April 1979, *Progr. Oceanogr.*, *12*, 87–145.

Figueiras, F. G., F. F. Perez, Y. Pazos, and A. F. Rios (1994), Light and productivity of Antarctic phytoplankton during austral summer in an ice edge region in the Weddell-Scotia Sea, *J. Plankt. Res.*, *16*, 233–254.

Fransson, A., M. Chierici, L. G. Anderson, I. Bussmann, G. Kattner, E. P. Jones, and J. H. Swift (2001), The importance of shelf processes for the modification of chemical constituents in the waters of the Eurasian Arctic Ocean: Implication for carbon fluxes, *Cont. Shelf Res.*, *21*, 225–242.

Gosselin, M., M. Levasseur, P. A. Wheeler, R. A. Horner, and B. C. Booth (1997), New measurements of phytoplankton and ice algal production in the Arctic Ocean, *Deep Sea Res.*, *44*, 1623–1644.

Grebmeier, J. M. (1993), Studies of pelagic-benthic coupling extended on to the Soviet continental shelf in the northern Bering and Chukchi Seas, *Cont. Shelf Res.*, *13*, 653–668.

Guay, C. K., G. P. Klinkhammer, K. K. Falkner, R. Benner, P. G. Coble, T. E. Whitledge, B. Black, F. J. Bussell, and T. A. Wagner (1999), High-

resolution measurements of dissolved organic carbon in the Arctic Ocean by in situ fiber-optic spectrometry, *Geophys. Res. Lett.*, *26*, 1007–1010.
Hansen, B., P. Verity, T. Falkenhaug, K. S. Tande, and F. Norrbin (1994), On the trophic fate of Phaeocystis pouchetii (Hariot). V. Trophic relationships between Phaeocystis and zooplankton: an assessment of methods and size dependence, *J. Plankt. Res.*, *16*, 487–511.
Henriksen, K., T. H. Blackburn, B. A. Lomstein, and C. P. McRoy (1993), Rates of nitrification,distribution of nitrifying bacteria and inorganic fluxes in norther Bering-Chukchi shelf sediments, *Cont. Shelf Res.*, *23*, 629–652.
Hollowed, A. B., and W. S. Wooster (1992), Variability of winter ocean conditions and strong year classes of Northeast Pacific groundfish, *ICES Mar. Sci. Symp.*, *195*, 433–444.
Howell-Kubler, A. N., E. J. Lessard, and J. M. Knapp (1996), Spring-time microprotozoan abundance and biomass in the southeastern Bering Sea and Shelikof Strait, Alaska, *J. Plankt. Res.*, *18*, 731–745.
Hunt, G. L., et al. (1999), The Bering Sea in 1998: The second consecutive year of extreme weather-forced anomalies, *Eos Trans. AGU*, *80*, 561, 565–566.
Johnson, M. A., A. Y. Proshutinsky, and I. V. Polyakov (1999), Atmospheric patterns forcing two regimes of Arctic circulation: a return to anticyclonic conditions?, *Geophys. Res. Lett.*, *26*, 1621–1624.
Keller, A. A., and U. Riebesell (1989), Phytoplankton carbon dynamics during a winter-spring diatom bloom in an enclosed marine ecosystem: Primary production, biomass, and loss rates, *Mar. Biol.*, *103*, 131–142.
Kelley, J. J., and D. W. Hood (1971), Carbon dioxide in the Pacific Ocean and Bering Sea: Upwelling and mixing, *J. Geophys. Res.*, *76*, 745–752.
Kerr, R. A. (1999), A new force in high-latitude climate, *Science*, *284*, 241–242.
Kinney, P. J., D. C. Burrell, M. E. Arheleger, T. C. Loder, and D. W. Hood (1970), Chukchi Sea data report: USCGC *Northwind*, July–August 1968; USCGC *Staten Island*, July–August 1969, *IMS Rep. R-70-23*, pp. 1–305, Univ. of Alaska, Fairbanks, Alaska.
Kistler, R., et al. (2001), The NCEP-NCAR 50 year reanalysis: Monthly means CD-ROM and documentation, *Bull Am. Meteorol. Soc.*, *82*, 247–267.
Leakey, R. J., N. Fenton, and A. Clarke (1994), The annual cycle of planktonic ciliates at Signy Island, Antarctica, *J. Plankt. Res.*, *16*, 841–856.
Macdonald, R. W. (1996), Arctic awakenings, *Nature*, *380*, 286-87.
Macdonald, R. W., M. O'Brien, E. C. Carmack, R. Pearson, F. A. McLaughlin, D. Sieberg, J. Barwell-Clarke, D. W. Paton, and D. Tuele (1995), Physical and chemical data collected in the Beaufort, Chukchi, and East Siberian Seas, August–September 1993, *Can. Data Rep. Hydrogr. Ocean Sci.*, *139*, 1-288.
Maslanik, J. A., M. C. Serreze, and R. G. Barry (1996), Recent decreases in Arctic summer ice cover and linkages to atmospheric circulation anomalies, *Geophys. Res. Lett.*, *23*, 1677–1680.
Maslowski, W., and W. H. Lipscomb (2003), High resolution simulations of Arctic sea ice, 1979–1993, *Polar Res.*, *22*, 67–74.
Maslowski, W., D. C. Marble, W. Walczowski, and A. J. Semtner (2001), On large scale shifts in the Arctic Ocean and sea ice conditions during 1979–1998, *Ann. Glaciol.*, *33*, 545–550.
Matrai, P. A., M. Vernet, R. Hood, A. Jennings, E. Brody, and S. Saemundsdottir (1995), Light-dependence of carbon and sulfur production by polar clones of the genus *Phaeocystis*, *Mar. Biol.*, *124*, 157–167.
McLaren, A. S., R. H. Bourke, J. E. Walsh, and R. L. Weaver (1994), Variability in sea-ice thickness over the North Pole from 1958 to 1992, in *The Polar Oceans and Their Role in Shaping the Global Environment*, *Geophys. Monogr. Ser.*, vol. 85, edited by O. M. Johannessen, R. D. Muench, and J. E. Overland, pp. 363–371, AGU, Washington, D.C.
McLaughlin, F. A., E. C. Carmack, R. W. Macdonald, and J. K. Bishop (1996), Physical and geochemical properties across the Atlantic/Pacific water mass front in the southern Canadian Basin, *J. Geophys. Res.*, *101*, 1183–1195.
McRoy, C. P. (1999), Water over the bridge: A summing up of the contributions of the ISHTAR project in the northern Bering and Chukchi Seas, in *Dynamics of the Bering Sea*, *Sea Grant AK-SG-03*, edited by T. R. Loughlin and K. Ohtani, pp. 687–696, Univ. of Alaska, Fairbanks, Alaska.
Millero, F. J., K. Lee, and M. Roche (1998), Distribution of alkalinity in the surface waters of the major oceans, *Mar. Chem.*, *60*, 111–130.
Muench, R. D., J. T. Gunn, T. E. Whitledge, P. Schlosser, and W. Smethie (2000), An Arctic Ocean cold core eddy, *J. Geophys. Res.*, *105*, 23,977–24,006.
Mumm, N., H. Auel, H. Hanssen, W. Hagen, C. Richter, and H. J. Hirche (1998), Breaking the ice: Large-scale distribution of mesozooplankton after a decade of Arctic and transpolar cruises, *Polar Biol.*, *20*, 189–197.
Murata, A., and T. Takizawa (2003), Summertime $CO_2$ sinks in shelf and slope waters of the western Arctic Ocean, *Cont. Shelf Res.*, *23*, 753–776.
Myneni, R. B., C. D. Keeling, C. J. Tucker, G. Asrar, and R. R. Nemani (1997), Increased plant growth in the northern high latitudes from 1981 to 1991, *Nature*, *386*, 698–702.
Niebauer, H. J. (1988), Effects of El Nino-Southern Oscillation and North Pacific weather patterns on interannual variability in the subarctic Bering Sea, *J. Geophys. Res.*, *93*, 5051–5068.
Olson, M. B., and S. L. Strom (2002), Phytoplankton growth, microzooplankton herbivory and community structure in the southeast Bering Sea: Insight into the formation and temporal persistence of the *Emiliana huxleyi* bloom, *Deep Sea Res.*, *49*, 5969–5990.
Overpeck, J., et al. (1997), Arctic environmental change of the last four centuries, *Science*, *278*, 1251–1256.
Palmisano, A. C., J. B. SooHoo, S. L. SooHoo, S. T. Kottmeier, L. L. Craft, and C. W. Sullivan (1986), Photoadaptation in *Phaeocystis pouchetii* advected beneath annual sea ice in McMurdo Sound, Antarctica. *J. Plankt. Res.*, *8*, 891–906.
Peng, T. H., T. Takahashi, W. S. Broecker, and J. Olafsson (1987), Seasonal variability of carbon dioxide, nutrients and oxygen in the northern North Atlantic surface water: Observations and a model, *Tellus, Ser. B*, *39*, 439–458.
Penta, B., and J. J. Walsh (1995), A one-dimensional ecological model of summer oxygen distributions within the Chukchi Sea, *Cont. Shelf Res.*, *15*, 337–356.
Perrin, R., P. Lu, and H. J. Marchant (1987), Seasonal variation in marine phytoplankton and ice algae at a shallow Antarctic coastal site, *Hydrobiologia*, *146*, 33–46.
Platt, T., W. G. Harrison, B. Irwin, E. P. Horne, and C. L. Gallegos (1982), Photosynthesis and photoadaptation of marine phytoplankton in the Arctic, *Deep Sea Res.*, *29*, 1159–1170.
Proshutinsky, A. Y., and M. A. Johnson (1997), Two circulation regimes of the wind-driven Arctic Ocean, *J. Geophys. Res.*, *102*, 12,493–12,514.
Reid, P. C., C. Lancelot, W. W. Gieskes, E. Hagmeier, and G. Weichart (1990), Phytoplankton of the North Sea and its dynamics: A review, *Neth. J. Sea Res.*, *26*, 295–331.
Rey, F. (1991), Photosynthesis-irradiance relationships in natural phytoplankton populations of the Barents Sea, *Polar Res.*, *10*, 105–116.
Roach, A. T., K. Aagaard, C. H. Pease, S. A. Salo, T. Weingartner, V. Pavlov, and M. Kulakov (1995), Direct measurements of transport and water properties through the Bering Strait, *J. Geophys. Res.*, *100*, 18,443–18,457.
Sakshaug, E. (2004), Primary production in the Arctic seas, in *The Organic Carbon Cycle in the Arctic Ocean: Present and Past*, edited by R. Stein, Springer-Verlag, New York, in press.
Sakshaug, E., and O. Holm-Hansen (1986), Photoadaptation in Antarctic phytoplankton: Variations in growth rate, chemical composition, and P versus I curves, *J. Plankt. Res.*, *8*, 459–473.
Sakshaug, E., and J. J. Walsh (2000), Marine biology: Biomass, productivity distributions and their variability in the Barents and Bering Seas, in *The Arctic: Environment, People, Policy*, edited by M. Nuttall and T. V. Callaghan, pp. 163–196, Harwood Acad., New York.
Sambrotto, R. N., and J. J. Goering (1983), Interannual variability of phytoplankton and zooplankton production on the southeast Bering Shelf, in *From Year to Year*, edited by W. S. Wooster, pp. 161–177, Sea Grant Publ., Univ. of Washington, Seattle, Wash.
Schell, D. M. (2000), Declining carrying capacity in the Bering Sea: Isotopic evidence from whale baleen, *Limnol. Oceanogr.*, *45*, 459–462.
Schell, D. M. (2001), Carbon isotope variations in Bering Sea biota: The role of anthropogenic carbon dioxide, *Limnol. Oceanogr.*, *46*, 999–1000.
Sherr, E. B., B. F. Sherr, and K. Thompson (2004), Annual cycle of autotrophic and hetrotrophic microbes in the upper water column of the central Arctic Ocean, *Deep Sea Res.*, in press.
Smith, J. N., S. B. Moran, and R. W. Macdonald (2003), Shelf-basin interactions in the Arctic Ocean based on $^{210}$Pb and Ra isotope tracer distributions, *Deep Sea Res.*, *50*, 397–416.
Smith, R., and P. Gent (Eds.) (2002), Reference manual for the parallel ocean program (POP): Ocean component of the Community Climate System Model (CCSM2.0), *Rep. LAUR-02-2484*, 74 pp., Los Alamos National Laboratory, Los Alamos, N. M.
Smith, W. O. (1995), Primary production and new production in the northeast water (Greenland) polynya during summer 1992, *J. Geophys. Res.*, *100*, 4357–4370.
Smith, W. O., L. A. Codispoti, D. M. Nelson, T. Manley, E. J. Buskey, H. J. Niebauer, and G. F. Cota (1991), Importance of Phaeocystis blooms in the high-latitude ocean carbon cycle, *Nature*, *352*, 514–516.
Springer, A. M., and C. P. McRoy (1993), The paradox of pelagic food webs in the northern Bering Sea. III. Patterns of primary production, *Cont. Shelf Res.*, *13*, 575–600.
Stabeno, P. J., and J. E. Overland (2001), Bering Sea shifts toward an earlier spring transition, *Eos Trans. AGU*, *82*, 317–321.

Stockwell, D. A., T. E. Whitledge, S. I. Zeeman, K. O. Coyle, J. N. Napp, R. D. Brodeur, A. I. Pinchuk, and G. L. Hunt (2001), Anomalous conditions in the south-eastern Bering Sea, 1997: Nutrients, phytoplankton and zooplankton, *Fish. Oceanogr.*, *10*, 99–116.

Stoddard, A., and J. J. Walsh (1986), Modeling oxygen depletion in the New York Bight: The water quality impact of a potential increase of waste inputs, in *Oceanic Processes in Marine Pollution*, vol. 5, *Urban Wastes in Coastal Marine Environments*, edited by D. A. Wolfe and T. P. O'Connor, pp. 91–102, Kreiger, Melbourne, Fla.

Sugimoto, T., and K. Tadokoro (1997), Interannual-interdecadal variations in zooplankton biomass, chlorophyll concentrations, and physical environment in the subarctic Pacific and Bering Sea, *Fish. Oceanogr.*, *6*, 74–93.

Sukhanova, I. N., H. J. Semina, and M. V. Venttsel (1999), Spatial distribution and temporal variability of phytoplankton in the Bering Sea, in *Dynamics of the Bering Sea*, *Sea Grant AK-SG-03*, edited by T. R. Loughlin and K. Ohtani, pp. 453–483, Univ. of Alaska, Fairbanks, Alaska.

Swift, J. H., E. P. Jones, K. Aagaard, E. C. Carmack, M. Hingston, R. W. Macdonald, F. A. McLaughlin, and R. G. Perkin (1997), Waters of the Makarov and Canada basins, *Deep Sea Res.*, *44*, 1503–1529.

Taylor, A. H., A. J. Watson, M. Ainsworth, J. E. Robertson, and D. R. Turner (1991), A modeling investigation of the role of phytoplankton in the balance of carbon at the surface of the North Atlantic, *Global Biogeochem. Cycles*, *5*, 151–172.

Thompson, D. W., and J. M. Wallace (1998), The Arctic Oscillation signature in the wintertime geopotential height and temperature fields, *Geophys Res. Lett.*, *25*, 1297–1300.

Verity, P. G., T. S. Smayda, and E. Sakshaug (1991), Photosynthesis, excretion, and growth rates of *Phaeocystis* colonies and solitary cells, *Polar Res.*, *10*, 117–129.

Vernet, M., P. A. Matrai, and I. Andeassen (1998), Synthesis of particulate and extracellular carbon by phytoplankton at the marginal ice zone in the Barents Sea, *J. Geophys. Res.*, *103*, 1023–1038.

Wadhams, P. (1997), Ice thickness in the Arctic Ocean: The statistical reliability of experimental data, *J. Geophys. Res.*, *102*, 27,951–27,960.

Wadhams, P. (2000), *Ice in the Ocean*, 351 pp., Gordon and Breach, Newark, N. J.

Walsh, J. J. (1989), Arctic carbon sinks: Present and future, *Global Biogeochem. Cycles*, *3*, 393–411.

Walsh, J. J. (1995), DOC storage in Arctic seas: the role of continental shelves, in *Arctic Oceanography: Marginal Ice Zones and Continental Shelves*, edited by W. O. Smith and J. M. Grebmeier, pp. 203–230, AGU, Washington D.C.

Walsh, J. J., and D. A. Dieterle (1994), $CO_2$ cycling in the coastal ocean. I. A numerical analysis of the southeastern Bering Sea, with applications to the Chukchi Sea and the northern Gulf of Mexico, *Progr. Oceanogr.*, *34*, 335–392.

Walsh, J. J., T. E. Whitledge, F. W. Barvenik, C. D. Wirick, S. O. Howe, W. E. Esaias, and J. T. Scott (1978), Wind events and food chain dynamics within the New York Bight, *Limnol. Oceanogr.*, *23*, 659–683.

Walsh, J. J., et al. (1989), Carbon and nitrogen cycling within the Bering/Chukchi Seas: Source regions of organic matter effecting AOU demands of the Arctic Ocean, *Progr. Oceanogr.*, *22*, 279–361.

Walsh, J. J., D. A. Dieterle, F. E. Muller-Karger, K. Aagaard, A. T. Roach, T. E. Whitledge, and D. A. Stockwell (1997), $CO_2$ cycling in the coastal ocean. II. Seasonal organic loading to the Canadian Basin from source waters south of Bering Strait, *Cont. Shelf Res.*, *17*, 1–36.

Walsh, J. J., D. A. Dieterle, and J. Lenes (2001), A numerical analysis of carbon dynamics of the Southern Ocean phytoplankton community: The roles of light and grazing in effecting both sequestration of atmospheric $CO_2$ and food availability to larval krill, *Deep Sea Res.*, *48*, 1–48.

Wassman, P., M. Vernet, B. G. Mitchell, and F. Rey (1990), Mass sedimentation of Phaeocystis pouchetii in the Barents Sea, *Mar. Ecol. Progr. Ser.*, *66*, 183–195.

Weingartner, T. J., D. J. Cavalieri, K. Aagaard, and Y. Sasaki (1998), Circulation, dense water formation, and outflow on the northeast Chukchi shelf, *J. Geophys. Res.*, *103*, 7647–7661.

Wheeler, P. A., J. M. Watkins, and R. L. Hansing (1997), Nutrients, organic carbon and organic nitrogen in the upper water column of the Arctic Ocean: Implications for the sources of dissolved organic carbon, *Deep Sea Res.*, *44*, 1571–1592.

Whitledge, T. E., W. S. Reeburgh, and J. J. Walsh (1986), Seasonal inorganic nitrogen distributions and dynamics in the southeastern Bering Sea, *Cont. Shelf Res.*, *5*, 109–132.

Zhang, Y., and E. C. Hunke (2001), Recent Arctic change simulated with a coupled ice-ocean model, *J. Geophys. Res.*, *106*, 4369–4390.

D. A. Dieterle and J. J. Walsh, College of Marine Science, University of South Florida, St. Petersburg, FL 33701, USA. (dwid@seas.marine.usf.edu; jwalsh@seas.marine.usf.edu)

W. Maslowski, Department of Oceanography, Naval Postgraduate School, Monterey, CA 93943, USA. (maslowsk@ucar.edu)

T. E. Whitledge, School of Fisheries and Ocean Sciences, University of Alaska, Fairbanks, AK 99775, USA. (terry@ims.uaf.edu)